



## Shear banding in large amplitude oscillatory shear (LAOStrain and LAOStress) of polymers and wormlike micelles

K. A. Carter, J. M. Girkin, and S. M. Fielding

Citation: *Journal of Rheology* **60**, 883 (2016); doi: 10.1122/1.4960512

View online: <http://dx.doi.org/10.1122/1.4960512>

View Table of Contents: <http://scitation.aip.org/content/sor/journal/jor2/60/5?ver=pdfcov>

Published by the [The Society of Rheology](#)

---

### Articles you may be interested in

[Understanding steady and dynamic shear banding in a model wormlike micellar solution](#)

*J. Rheol.* **60**, 1001 (2016); 10.1122/1.4961035

[Shear banding in time-dependent flows of polymers and wormlike micelles](#)

*J. Rheol.* **58**, 103 (2014); 10.1122/1.4842155

[Large amplitude oscillatory shear \(LAOS\) measurements to obtain constitutive equation model parameters: Giesekus model of banding and nonbanding wormlike micelles](#)

*J. Rheol.* **56**, 333 (2012); 10.1122/1.3684751

[Yielding processes in a colloidal glass of soft star-like micelles under large amplitude oscillatory shear \(LAOS\)](#)

*J. Rheol.* **54**, 1219 (2010); 10.1122/1.3483610

[Investigation of shear-banding structure in wormlike micellar solution by point-wise flow-induced birefringence measurements](#)

*J. Rheol.* **49**, 537 (2005); 10.1122/1.1849179

---

## The World's Most Versatile Platform for Rheological Measurements



The Discovery  
Hybrid Rheometer  
from



# Shear banding in large amplitude oscillatory shear (LAOStrain and LAOStress) of polymers and wormlike micelles

K. A. Carter,<sup>a)</sup> J. M. Girkin, and S. M. Fielding

*Department of Physics, Durham University, Science Laboratories, South Road, Durham DH1 3LE, United Kingdom*

(Received 1 October 2015; final revision received 1 April 2016; published 12 September 2016)

## Abstract

We investigate theoretically shear banding in large amplitude oscillatory shear (LAOS) of polymeric and wormlike micellar surfactant fluids. In large amplitude oscillatory shear strain, we observe banding at low frequencies and sufficiently high strain rate amplitudes in fluids for which the underlying stationary constitutive curve of shear stress as a function of shear rate is nonmonotonic. This is the direct (and relatively trivial) analog of quasisteady state banding seen in slow strain rate sweeps along the flow curve. At higher frequencies and sufficiently high strain amplitudes, we report a different but related phenomenon, which we call “elastic” shear banding. This is associated with an overshoot in the elastic (Lissajous–Bowditch) curve of stress as a function of strain and we suggest that it might arise rather widely even in fluids that have a monotonic underlying constitutive curve, and so do not show steady state banding if under a steadily applied shear flow. It is analogous to the elastic banding triggered by stress overshoot in a fast shear startup predicted previously by R. L. Moorcroft and S. M. Fielding [Phys. Rev. Lett. **110**(8), 086001 (2013)], but could be more readily observable experimentally in this oscillatory protocol due to its recurrence in each half cycle. In large amplitude oscillatory shear stress, we report shear banding in fluids that shear thin strongly enough to have either a negatively or a weakly positively sloping region in the underlying constitutive curve, noting again that fluids in the latter category do not display steady state banding in a steadily applied flow. This banding is triggered in each half cycle as the stress magnitude transits the region of weak slope in an upward direction such that the fluid effectively yields. It is strongly reminiscent of the transient banding predicted previously in step stress [R. L. Moorcroft and S. M. Fielding, Phys. Rev. Lett. **110**(8), 086001 (2013)]. Our numerical calculations are performed in the Rolie-poly model of polymers and wormlike micelles, but we also provide arguments suggesting that our results should apply more widely. Besides banding in the shear strain rate profile, which can be measured by velocimetry, we also predict banding in the shear and normal stress components, measurable by birefringence. As a backdrop to understanding the new results on shear banding in LAOS, we also briefly review earlier work on banding in other time-dependent protocols, focusing in particular on shear startup and step stress. © 2016 The Society of Rheology. [<http://dx.doi.org/10.1122/1.4960512>]

## I. INTRODUCTION

Many complex fluids display shear banding, in which a state of initially homogeneous shear flow gives way to the formation of coexisting bands of differing shear rate, with layer normal in the flow-gradient direction. For recent reviews, see [1–4]. Following its early observation in wormlike micellar surfactant solutions [5], over the past two decades shear banding has been seen in virtually all the major classes of complex fluids and soft solids. Examples include microgels [6], clays [7], emulsions [8] foams [9], lamellar surfactant phases [10], triblock copolymers [11,12], star polymers [13], and—subject to ongoing controversy [14–20]—linear polymers.

Prior to about 2010, the majority of studies of shear banding focused on conditions of a steadily applied shear flow. The criterion for the presence of steady state banding in this case is well known: That the underlying homogeneous constitutive curve of shear stress as a function of shear rate has a regime of negative slope. (In some cases of strong concentration, coupling shear banding can arise even for a monotonic constitutive curve [21], but we do not consider that case here.) Such a regime is predicted by the original tube theory

of Doi and Edwards for nonbreakable polymers [22], and by the reptation-reaction model of wormlike micellar surfactants [23]. It is straightforward to show that a state of initially homogeneous shear flow is linearly unstable, in this regime of negative constitutive slope, to the formation of shear bands [24]. The composite steady state flow curve of shear stress as a function of shear rate then displays a characteristically flat plateau regime, in which shear bands are observed.

From an experimental viewpoint, the evidence for steady state shear banding under a steadily applied shear flow is now overwhelming in the case of wormlike micelles. For reviews, see [25,26]. For linear unbreakable polymers, the issue remains controversial, as recently reviewed in [27]. In particular, the original Doi–Edwards model did not account for a process known as convective constraint release (CCR) [28–30]. Since CCR (which we describe below) was proposed, there has been an ongoing debate about its efficacy in potentially eliminating the regime of negative constitutive slope and restoring a monotonic constitutive curve, thereby eliminating steady state banding. However, a nonmonotonic constitutive curve and associated steady state shear banding has been seen in molecular dynamics simulations of polymers [31], for long enough chain lengths. It is important to note, though, that the polydispersity that is often present in practice in unbreakable polymers also tends to restore monotonicity.

<sup>a)</sup>Author to whom correspondence should be addressed; electronic mail: [k.a.carter@durham.ac.uk](mailto:k.a.carter@durham.ac.uk)

Besides the conditions of steady state flow just described, many flows of practical importance involve a strong time dependence. In view of this, a natural question to ask is whether shear banding might also arise in these time-dependent flows and, if so, under what conditions. Over the past decade, a body of experimental data has accumulated to indicate that it does indeed occur: In shear startup [6,7,16,32–34], following a step strain (in practice a rapid strain ramp) [35–41], and following a step stress [14,33,34,41–46].

Consistent with this growing body of experimental evidence, theoretical considerations [47–51] also suggest that shear banding might arise rather generically in flows with a sufficiently strong time dependence, even in fluids that have a monotonically increasing constitutive curve and so do not display steady state banding under conditions of a continuously applied shear. Indeed, the calculations to date suggest that the set of fluids that show banding in steady state is only a subset of those that exhibit banding in time-dependent flows. In view of this, although the question concerning the existence or otherwise of steady state shear banding in polymers remains an important one, the resolution of that controversy is likely to be of less practical importance to the broader issue of whether shear banding arises more generally in time-dependent flows.

In the last five years, progress has been made in establishing theoretically, separately for each of the time-dependent flow protocols listed above (shear startup, step strain, and step stress), a fluid-universal criterion [47] for the onset of shear banding, based on the shape of the time-dependent rheological response function for the particular protocol in question. We now briefly review these criteria as backdrop to understanding the results that follow below for shear banding in large amplitude oscillatory shear (LAOS).

In shear startup (the switch-on at some time  $t=0$  of a constant shear rate  $\dot{\gamma}$ ), the onset of banding is closely associated with the presence of an overshoot [47–51] in the startup signal of stress as a function of time (or equivalently as a function of strain), as it evolves toward its eventual steady state on the material's flow curve. This concept builds on the early insight of [52]. The resulting bands may, or may not, then persist to steady state, according to whether or not the underlying constitutive curve of stress as a function of strain rate is nonmonotonic. This tendency of a startup overshoot to trigger banding was predicted on the basis of fluid-universal analytical calculations in [47], and has been confirmed in numerical simulations of polymeric fluids (polymer solutions, polymer melts, and wormlike micelles) [48,50], polymer glasses [53], and soft glassy materials (SGMs) (dense emulsions, microgels, foams, etc.) [49,51,54]. It is consistent with experimental observations in wormlike micellar surfactants [41,44], polymers [14,16,33,34,36,55–57], carbopol gels [6,32], and Laponite clay suspensions [7].

Following the imposition of a step stress in a previously undeformed sample, the onset of shear banding is closely associated with the existence of a regime of simultaneous upward slope and upward curvature in the time-differentiated creep response curve of shear rate as a function of time [3,47]. This criterion was also predicted on the basis of fluid-universal analytical calculations in [47], and has been confirmed in

numerical simulations of polymeric fluids [48] and SGMs [3]. It is consistent with experimental observations in polymers [14,33,34,41,44–46,57], carbopol microgels [43], and carbon black suspensions [42].

In the shear startup and step stress experiments just described, the time dependence is inherently transient in nature: After (typically) several strain units, the system evolves to its eventual steady state on the material's flow curve. In any such protocol, for a fluid with a monotonic constitutive curve that precludes steady state banding, any observation of banding is predicted to be limited to this regime of time dependence following the inception of the flow. That poses an obvious technical challenge to experimentalists: Of imaging the flow with sufficient time resolution to detect these transient bands. This is particularly true for a polymeric fluid with a relatively fast relaxation spectrum. For SGMs, in contrast, the dynamics are typically much slower and any bands associated with the onset of flow, though technically transient, may persist for a sufficiently long time to be mistaken for the material's ultimate steady state response for any practical purpose [3,49].

In the past decade, the rheological community has devoted considerable attention to the study of LAOS. For a recent review, see [58]. In this protocol, the applied flow has the form of a sustained oscillation and is therefore perpetually time dependent, in contrast to the transient time dependence of the shear startup and step stress protocols just described. But by analogy with the predictions of transient shear banding in shear startup and step stress, a sustained oscillatory flow might (in certain regimes that we shall discuss) be expected to repeatedly show banding at certain phases of the cycle, or even to show sustained banding round the whole cycle. Importantly, again by analogy with our knowledge of shear startup and step stress, this effect need not be limited to fluids with a nonmonotonic constitutive curve that shows steady state banding in a continuously applied shear flow, but might instead arise as a natural consequence of the time dependence inherent in the oscillation.

Indeed, a particularly attractive feature of LAOS is that the severity of the flow's time dependence, relative to the fluid's intrinsic characteristic relaxation timescale  $\tau$ , can be tuned by varying the frequency  $\omega$  of the applied oscillation. A series of LAOS experiments can thereby explore the full range between steady state behavior in the limit  $\omega \rightarrow 0$ , where the oscillation effectively corresponds to a repeated series of quasistatic sweeps up and down the flow curve, and strongly time-dependent behavior for  $\omega > 1/\tau$ . A fluid with a nonmonotonic underlying constitutive curve that admits steady state banding is then clearly expected to exhibit banding in the limit of  $\omega \rightarrow 0$ , as the shear rate quasistatically transits the plateau in the steady state flow curve. In contrast, a monotonic constitutive curve precludes banding for  $\omega \rightarrow 0$ . Crucially, though, as noted above, the absence of banding in steady state conditions does not rule out the possibility of banding in flows with a strong enough time dependence,  $\omega \gtrsim O(1/\tau)$ .

Indeed, intuitively, a square-wave caricature of a large amplitude oscillatory shear strain (LAOS<sub>strain</sub>) experiment points to a perpetual switching between a shear startuplate

process in the forward direction, followed by “reverse startup” in the opposite direction. Any regime in which these startuplike events are associated with an overshoot in the associated curve of stress as a function of strain then strongly suggests the possibility of shear banding during those quasistartup parts of the cycle, by analogy with the criterion for banding in a true shear startup from rest. In the same spirit, a square-wave caricature of a large amplitude oscillatory shear stress (LAOStress) experiment indicates a perpetually repeated series of step stress events, jumping between positive and negative stress values, and so admitting the possibility of shear banding if the criterion for banding following a step stress is met.

In practice, of course, LAOS is more complicated than the caricatures just described and the criteria for banding in shear startup and step stress might only be expected to apply in certain limiting regimes. Nonetheless, in what follows we shall show that many of our results for banding in LAOStrain and LAOStress can, to a large extent, be understood within the framework of these existing criteria for the simpler time-dependent protocols.

Experimentally, shear banding has indeed been observed in LAOS: In polymer solutions [15], dense colloids [59], and also in wormlike micellar surfactants that are known to shear band in steady state [60–62].

From a theoretical viewpoint, several approaches to the interpretation of LAOS data have been put forward in the literature [58]. These include Fourier transform rheology [63]; measures for quantifying Lissajous–Bowditch curves (defined below) in their elastic representation of stress versus strain, or viscous representation of stress versus strain rate [64]; a decomposition into characteristic sine, square, and triangular wave prototypical response functions [65,66]; decomposition into elastic and viscous stress contributions using symmetry arguments [67]; Chebyshev series expansions of these elastic and viscous contributions [68]; and interpretations of the LAOS cycle in terms of a sequence of physical processes (SPP) [69,70].

However, many of these existing theoretical studies assume either explicitly or implicitly that the flow remains homogeneous, and thereby fail to take account of the possibility of shear banding. An early exception can be found in [71,72], which studied a model of wormlike micellar surfactants with a nonmonotonic constitutive curve in LAOStrain. Another exception is in the paper of Adams and Olmsted [73], which recognized that shear banding can arise even in the absence of any nonmonotonicity in the underlying constitutive curve.

The work that follows here builds on the remarkable insight of these early papers, in carrying out a detailed numerical study of shear banding in LAOStrain and LAOStress within the Rolie-poly (RP) model [74] of polymers and wormlike micellar surfactant solutions. Consistent with the above discussion, in LAOStrain we observe banding at low frequencies  $\omega \rightarrow 0$  and sufficiently high strain rate amplitudes  $\dot{\gamma} \gtrsim 1/\tau$  in fluids for which the underlying constitutive curve of shear stress as a function of shear rate is nonmonotonic. At higher frequencies  $\omega = O(1/\tau)$  and for sufficiently high strain amplitudes  $\gamma \gtrsim 1$ , we instead see

“elastic” shear banding associated with an overshoot in the elastic curve of stress as a function of strain, in close analogy with the elastic banding predicted in a fast shear startup experiment [47,48,50,73]. Importantly, we show that this elastic banding arises robustly even in a wide range of model parameter space for which the underlying constitutive curve is monotonic, precluding steady state banding.

In LAOStress, we observe banding in fluids that shear thin sufficiently strongly to have either a negatively, or weakly positively, sloping region in the underlying constitutive curve. We emphasize again that fluids in the latter category do not display steady state banding, and therefore that, for such fluids, the banding predicted in LAOStress is a direct result of the time dependence of the applied flow. In this case, the banding is triggered in each half cycle as the stress magnitude transits in an upward direction the region of weak slope and the strain rate magnitude increases dramatically such that the material effectively yields. This is strongly reminiscent of the transient banding discussed previously in step stress [47,48].

While it would be interesting to interpret our findings within one (or more) of the various mathematical methodologies for analyzing LAOS discussed above (and in particular to consider the implications of banding for the presence of higher harmonics in the output rheological time series), in the present manuscript we focus instead on the physical understanding that can be gained by considering the shapes of the signals of stress versus strain or strain rate (in LAOStrain) and strain rate versus time (in LAOStress). In that sense, this work is closest in spirit to the SPP approach of [69,70] (which did not, however, explicitly consider heterogeneous response). In particular, we seek to interpret the emergence of shear banding in LAOS on the basis of the existing criteria for the onset of banding in the simpler time-dependent protocols of shear startup and step stress [47].

The paper is structured as follows. In Sec. II, we introduce the model, flow geometry, and protocols to be considered. Section III outlines the calculational methods that we shall use. Section IV contains a summary of previously derived linear instability criteria for shear banding in steady shear, fast shear startup, and step shear stress protocols, with the aim of providing a backdrop to understanding shear banding in oscillatory protocols. In Secs. V and VI, we present our results for LAOStrain and LAOStress, respectively, and discuss their potential experimental verification. Finally, Sec. VII contains our conclusions and an outlook for future work.

## II. MODEL, FLOW GEOMETRY, AND PROTOCOLS

We write the stress  $\Sigma(\mathbf{r}, t)$  at any time  $t$  in a fluid element at position  $\mathbf{r}$  as the sum of a viscoelastic contribution  $\sigma(\mathbf{r}, t)$  from the polymer chains or wormlike micelles, a Newtonian contribution characterized by a viscosity  $\eta$ , and an isotropic contribution with pressure  $p(\mathbf{r}, t)$

$$\Sigma = \sigma + 2\eta\mathbf{D} - p\mathbf{I}. \quad (1)$$

The Newtonian stress  $2\eta\mathbf{D}(\mathbf{r}, t)$  may arise from the presence of a true solvent, and from any polymeric degrees of freedom

considered fast enough not to be ascribed their own viscoelastic dynamics. The symmetric strain rate tensor  $\mathbf{D} = (1/2)(\mathbf{K} + \mathbf{K}^T)$  where  $K_{\alpha\beta} = \partial_\beta v_\alpha$  and  $\mathbf{v}(\mathbf{r}, t)$  is the fluid velocity field.

We consider the zero Reynolds number limit of creeping flow, in which the condition of local force balance requires the stress field  $\Sigma(\mathbf{r}, t)$  to be divergence free

$$\nabla \cdot \Sigma = 0. \quad (2)$$

The pressure field  $p(\mathbf{r}, t)$  is determined by enforcing that the flow remains incompressible

$$\nabla \cdot \mathbf{v} = 0. \quad (3)$$

The viscoelastic stress is then written in terms of a constant elastic modulus  $G$  and a tensor  $\mathbf{W}(\mathbf{r}, t)$  characterising the conformation of the polymer chains or wormlike micelles,  $\boldsymbol{\sigma} = G(\mathbf{W} - \mathbf{I})$ . We take the dynamics of  $\mathbf{W}$  to be governed by the RP model [74] with

$$\begin{aligned} \partial_t \mathbf{W} + \mathbf{v} \cdot \nabla \mathbf{W} &= \mathbf{K} \cdot \mathbf{W} + \mathbf{W} \cdot \mathbf{K}^T - \frac{1}{\tau_d} (\mathbf{W} - \mathbf{I}) \\ &\quad - \frac{2(1-A)}{\tau_R} [\mathbf{W} + \beta A^{-2\delta} (\mathbf{W} - \mathbf{I})] \\ &\quad + D \nabla^2 \mathbf{W}, \end{aligned} \quad (4)$$

in which  $A = \sqrt{3/T}$  with trace  $T = \text{tr } \mathbf{W}$ . This RP model is a single mode simplification of the GLAMM model [75], which provides a microscopically derived stochastic equation for the dynamics of a test chain (or micelle) in its mean field tube of entanglements with other chains. The timescale  $\tau_d$  sets the characteristic time on which a chain escapes its tube by means of 1D curvilinear diffusion along the tube's contour, known as reptation, allowing the molecular orientation to refresh itself. The Rouse timescale  $\tau_R$  sets the shorter time on which chain stretch, as characterized by  $T = \text{tr } \mathbf{W}$ , relaxes. The ratio  $\tau_d/\tau_R = 3Z$ , where  $Z$  is the number of entanglements per chain. The parameters  $\beta$  and  $\delta$  govern a phenomenon known as CCR [28–30], in which the relaxation of the stretch of a test chain has the effect of also relaxing entanglement points, thereby facilitating the relaxation of tube orientation. The diffusive term  $D \nabla^2 \mathbf{W}$  added to the right-hand side of Eq. (4) is required to account for the slightly diffuse nature of the interface between shear bands [76]: Without it, the shear rate would be discontinuous across the interface, which is unphysical.

Using this model, we will consider shear flow between infinite flat parallel plates at  $y = \{0, L\}$ , with the top plate moving in the  $\hat{x}$  direction at speed  $\dot{\gamma}(t)L$ . We assume translational invariance in the flow direction  $\hat{x}$  and vorticity direction  $\hat{z}$  such that the fluid velocity can be written as  $\mathbf{v} = v(y, t)\hat{x}$ . The local shear rate at any position  $y$  is then given by

$$\dot{\gamma}(y, t) = \partial_y v(y, t), \quad (5)$$

and the spatially averaged shear rate

$$\bar{\dot{\gamma}}(t) = \frac{1}{L} \int_0^L \dot{\gamma}(y, t) dy. \quad (6)$$

Such a flow automatically satisfies the constraint of incompressibility, Eq. (3). The force balance condition, Eq. (2), further demands that the total shear stress is uniform across the cell, in the planar flow situation considered here, giving  $\partial_y \Sigma_{xy} = 0$ . The viscoelastic and Newtonian contributions may, however, each depend on space provided their sum remains uniform

$$\Sigma_{xy}(t) = G W_{xy}(y, t) + \eta \dot{\gamma}(y, t). \quad (7)$$

For such a flow, the RP model can be written component-wise as

$$\begin{aligned} \dot{W}_{xy} &= \dot{\gamma} W_{yy} - \frac{W_{xy}}{\tau_d} - \frac{2(1-A)}{\tau_R} (1 + \beta A) W_{xy} + D \partial_y^2 W_{xy}, \\ \dot{W}_{yy} &= -\frac{W_{yy} - 1}{\tau_d} - \frac{2(1-A)}{\tau_R} [W_{yy} + \beta A (W_{yy} - 1)] + D \partial_y^2 W_{yy}, \\ \dot{T} &= 2\dot{\gamma} W_{xy} - \frac{T - 3}{\tau_d} - \frac{2(1-A)}{\tau_R} [T + \beta A (T - 3)] + D \partial_y^2 T. \end{aligned} \quad (8)$$

(The other components of  $\mathbf{W}$  decouple to form a separate equation set, with trivial dynamics.) In the limit of fast chain stretch relaxation  $\tau_R \rightarrow 0$ , we obtain the simpler “nonstretching” RP model in which the trace  $T = 3$  and

$$\begin{aligned} \dot{W}_{xy} &= \dot{\gamma} \left[ W_{yy} - \frac{2}{3} (1 + \beta) W_{xy}^2 \right] - \frac{1}{\tau_d} W_{xy} + D \partial_y^2 W_{xy}, \\ \dot{W}_{yy} &= \frac{2}{3} \dot{\gamma} [\beta W_{xy} - (1 + \beta) W_{xy} W_{yy}] - \frac{1}{\tau_d} (W_{yy} - 1) + D \partial_y^2 W_{yy}. \end{aligned} \quad (9)$$

For convenient shorthand, we shall refer to this simpler nonstretching form as the nRP model. We refer to the full “stretching” model of Eq. (8) as the sRP model.

For boundary conditions at the walls of the flow cell, we assume no slip and no permeation for the fluid velocity, and zero gradient  $\partial_y W_{\alpha\beta} = 0$  for every component  $\alpha\beta$  of the polymeric conformation tensor.

In what follows, we consider the behavior of the RP model in the following two flow protocols:

- LAOStrain, with an imposed strain

$$\gamma(t) = \gamma_0 \sin(\omega t), \quad (10)$$

to which corresponds the strain rate

$$\dot{\gamma}(t) = \gamma_0 \omega \cos(\omega t) = \dot{\gamma}_0 \cos(\omega t). \quad (11)$$

- LAOStress, with an imposed stress

$$\Sigma(t) = \Sigma_0 \sin(\omega t). \quad (12)$$

The model, flow geometry, and protocol just described are characterized by the following parameters: The polymer

modulus  $G$ , the reptation timescale  $\tau_d$ , the stretch relaxation timescale  $\tau_R$ , the CCR parameters  $\beta$  and  $\delta$ , the stress diffusivity  $D$ , the solvent viscosity  $\eta$ , the gap size  $L$ , the frequency  $\omega$ , and the amplitude  $\gamma_0$  (for LAOStrain) or  $\Sigma_0$  (for LAOStress). We are free to choose units of mass, length, and time, thereby reducing the list by three: We work in units of length in which the gap size  $L = 1$ , of time in which the reptation time  $\tau_d = 1$  and of mass (or actually stress) in which the polymer modulus  $G = 1$ . We then set the value of the diffusion constant  $D$  such that the interface between the bands has a typical width  $\ell = \sqrt{D\tau_d} = 2 \times 10^{-2}L$ , much smaller than the gap size. This is the physically relevant regime for the macroscopic flow cells of interest here, and we expect the results we report to be robust to reducing  $l$  further. Following [74], we set  $\delta = -1/2$ .

Adimensional quantities remaining to be explored are then the model parameters  $\eta$ ,  $\beta$ , and (for the sRP model only)  $\tau_R$ ; and the protocol parameters  $\omega$  and  $\gamma_0$  or  $\Sigma_0$ . For each set of model parameters, we explore the whole plane of feasibly accessible values of protocol parameters  $\omega$  and  $\gamma_0$  or  $\Sigma_0$ .

Among the model parameters, the CCR parameter has the range  $0 \leq \beta \leq 1$ . Within this, there is no current consensus as to its precise value, and we shall therefore explore widely the full range  $0 \rightarrow 1$ . For the fluids of interest, here the Newtonian viscosity is typically much smaller than the zero shear viscosity of the viscoelastic component, giving  $\eta \ll 1$  in our units. Based on a survey of the experimental data, a range of  $10^{-7}$ – $10^{-3}$  was suggested by Graham *et al.* in [77]. Consistent with comments made in [78], we find values less than  $10^{-5}$  unfeasible to explore numerically, due to a resulting large separation of timescales between  $\tau_d$  and  $\eta/G$ . Therefore we adopt typical values  $\eta = 10^{-4}$  and  $10^{-5}$ . Given that the susceptibility to shear banding increases with decreasing  $\eta$ , we note that the levels of banding reported in what follows are likely, if anything, to be an underestimate of what might be observed experimentally. We return in our concluding remarks to discuss this issue further.

We explore a wide range of values of the stretch relaxation time  $\tau_R$ , or equivalently of the degree of entanglement  $Z = \tau_d/3\tau_R$ : We consider  $Z = 1$  to 350 for the sRP model (and note that the nRP model has  $Z \rightarrow \infty$  by definition). Experimentally, values of  $Z$  in the range of 50 appear commonplace and 100 toward the upper end of what might currently be used experimentally in nonlinear rheological studies. One of the objectives of this work is to provide a roadmap of values of  $Z$  and  $\beta$  in which shear banding is expected to be observed, for typical small values of  $\eta$ , in a sequence of LAOS protocols that scan amplitude and frequency space.

### III. CALCULATION METHODS

In this section, we outline the theoretical methods to be used throughout the paper. In order to develop a generalized framework encompassing both the nRP and sRP models, we combine all the relevant dynamical variables (for any given model) into a state vector  $s$ , with  $s = (W_{xy}, W_{yy})^T$  for the

nRP model and  $s = (W_{xy}, W_{yy}, T)^T$  for the sRP model. Alongside this, we define a projection vector  $p$  of corresponding dimensionality  $d$ , with  $p = (1, 0)$  for the nRP model and  $p = (1, 0, 0)$  for sRP.

The total shear stress  $\Sigma_{xy} = \Sigma$ , from which we drop the  $xy$  subscript for notational brevity, is then given by

$$\Sigma(t) = Gp \cdot s(y, t) + \eta \dot{\gamma}(y, t), \quad (13)$$

and the viscoelastic constitutive equation has the generalized form

$$\partial_t s(y, t) = Q(s, \dot{\gamma}) + D \partial_y^2 s. \quad (14)$$

The dimensionality and functional form of  $Q$  then specify the particular constitutive model. In this way, our generalized notation in fact encompasses not only the nRP model (for which  $d = 2$ ) and sRP model (for which  $d = 3$ ) but many more besides, including the Johnson Segalman, Giesekus, and Oldroyd B models [79].

#### A. Homogeneous base state

For any given applied flow, our approach will be first to calculate the fluid's response within the simplifying assumption that the deformation must remain homogeneous across the cell. While this is an artificial (and indeed incorrect) constraint in any regime where shear banding is expected, it nonetheless forms an important starting point for understanding the mechanism by which shear banding sets in. (We also note that most papers in the literature make this assumption throughout, thereby disallowing any possibility of shear banding altogether.)

Within this assumption of homogeneous flow, the response of the system follows as the solution to the set of ordinary differential equations

$$\hat{\Sigma}(t) = Gp \cdot \hat{s}(t) + \eta \hat{\dot{\gamma}}(t), \quad (15)$$

and

$$\hat{\dot{s}}(t) = Q(\hat{s}, \hat{\dot{\gamma}}). \quad (16)$$

In these either  $\hat{\dot{\gamma}}(t)$  or  $\hat{\Sigma}(t)$  is imposed, in LAOStrain and LAOStress, respectively, and the other dynamical quantities are calculated numerically using an explicit Euler algorithm [80]. We use the “hat” notation to denote that the state being considered is homogeneous.

#### B. Linear stability analysis

Having calculated the behavior of the fluid within the assumption that the flow remains homogeneous, we now proceed to consider whether this homogeneous “base state” flow will, at any point during an applied oscillatory protocol, be unstable to the formation of shear bands. To do so, we add to the base state, for which we continue to use the hat notation, heterogeneous perturbations of (initially) small amplitude

$$\begin{aligned}\Sigma(t) &= \hat{\Sigma}(t), \\ \dot{\gamma}(y, t) &= \hat{\dot{\gamma}}(t) + \sum_{n=1}^{\infty} \delta\dot{\gamma}_n(t) \cos(n\pi y/L), \\ s(y, t) &= \hat{s}(t) + \sum_{n=1}^{\infty} \delta s_n(t) \cos(n\pi y/L).\end{aligned}\quad (17)$$

Note that the total stress,  $\Sigma$ , is not subject to heterogeneous perturbations because the constraint of force balance decrees that it must remain uniform across the gap, at least in a planar shear cell. Substituting Eq. (17) into Eqs. (13) and (14), and expanding in successive powers of the magnitude of the small perturbations  $\delta\dot{\gamma}_n$ ,  $\delta s_n$ , we recover at zeroth order Eqs. (15) and (16) for the dynamics of the base state. At first order, the heterogeneous perturbations obey

$$\begin{aligned}0 &= G\mathbf{p} \cdot \delta s_n(t) + \eta\delta\dot{\gamma}_n(t), \\ \dot{\delta s}_n &= \mathbf{M}(t) \cdot \delta s_n + \mathbf{q}\delta\dot{\gamma}_n,\end{aligned}\quad (18)$$

in which  $\mathbf{M} = \partial_s \mathbf{Q}|_{s, \dot{\gamma}} - \delta D(n\pi/L)^2$  and  $\mathbf{q} = \partial_{\dot{\gamma}} \mathbf{Q}|_{s, \dot{\gamma}}$ . Combining these gives

$$\dot{\delta s}_n = \mathbf{P}(t) \cdot \delta s_n, \quad (19)$$

with

$$\mathbf{P}(t) = \mathbf{M}(t) - \frac{G}{\eta} \mathbf{q}(t) \mathbf{p}. \quad (20)$$

In any regime where the heterogeneity remains small, terms of second order and above can be neglected.

To determine whether at any time  $t$  during an imposed oscillatory flow the heterogeneous perturbations  $\delta\dot{\gamma}_n$ ,  $\delta s_n(t)$  have positive rate of growth, indicating linear instability of the underlying homogeneous base state to the onset of shear banding, we consider first of all the instantaneous sign of the eigenvalue  $\lambda(t)$  of  $\mathbf{P}(t)$  that has the largest real part. A positive value of  $\lambda(t)$  is clearly suggestive that heterogeneous perturbations will be instantaneously growing at that time  $t$ . We note, however, that the concept of a time-dependent eigenvalue must be treated with caution. In view of this, we cross check predictions made on the basis of the eigenvalue by also directly numerically integrating the linearized Eq. (19) using an explicit Euler algorithm. This allows us to determine unambiguously whether the heterogeneous perturbations will be at any instant growing (taking the system toward a banded state) or decaying (restoring a homogeneous state), at the level of this linear calculation.

In these linear stability calculations, we neglect the diffusive term in the viscoelastic constitutive equation, setting  $D=0$ . Reinstating it would simply transform any eigenvalue  $\lambda \rightarrow \lambda_n = \lambda - Dn^2\pi^2/L^2$  and provide a mechanism whereby any heterogeneity with a wavelength of order the microscopic length scale  $l$ , or below, diffusively decays. Accordingly, the results of this linear calculation only properly capture the dynamics of any heterogeneous perturbations that have macroscopically large wavelengths, which are the ones of interest in determining the initial formation of shear bands starting from a homogeneous base state.

As a measure of the degree of flow heterogeneity at any time  $t$  in this linear calculation, we shall report in our results sections  $\delta\dot{\gamma}(t)$  is normalized by the amplitude of the imposed oscillation  $\dot{\gamma}_0$  in LAOStrain, or by  $1 + |\dot{\gamma}(t)|$  in LAOStress, where  $\dot{\gamma}(t)$  is the instantaneous value of the shear rate. (We find numerically that bands tend to form in LAOStress when  $|\dot{\gamma}(t)| \gg 1$ . The additional 1 in the normalization is used simply to prevent the divergence of this measure when  $\dot{\gamma}(t)$  passes through 0 in each half cycle.) Note that we no longer need to specify the mode number  $n$  for  $\delta\dot{\gamma}$  because within the assumption  $D=0$  just described, we are confining our attention to the limit of long wavelength modes only and noting them all to have the same dynamics, to within small corrections set by  $D$ .

### C. Full nonlinear simulation

While the linear analysis just described provides a calculationally convenient method for determining whether shear banding will arise in any given oscillatory measurement, enabling us to quickly build up an overall roadmap of parameter space, it cannot predict the detailed dynamics of the shear bands once the amplitude of heterogeneity has grown sufficiently large that nonlinear effects are no longer negligible. Therefore in what follows we shall also perform full nonlinear simulations of the model's spatiotemporal dynamics by directly integrating the full model Eqs. (13) and (14) using a Crank–Nicolson algorithm [80], with the system's state discretized on a grid of  $J$  values of the spatial coordinate  $y$ , checked in all cases for convergence with respect to increasing the number of grid points.

As a measure of the degree of shear banding at any time  $t$  in this nonlinear calculation, we report the difference between the maximum and minimum values of the shear rate across the cell

$$\Delta\dot{\gamma}(t) = \frac{1}{N} [|\dot{\gamma}_{\max}(t) - \dot{\gamma}_{\min}(t)|], \quad (21)$$

again normalized depending upon the employed protocol, by  $N$ , where  $N$  is the amplitude of the imposed oscillation  $\dot{\gamma}_0$  in LAOStrain, and  $1 + |\dot{\gamma}(t)|$  in LAOStress.

### D. Seeding the heterogeneity

When integrating the model equations to determine the time evolution of any flow heterogeneity, whether linearized or in their full nonlinear form, we must also specify the way in which whatever heterogeneous perturbations that are the precursor to the formation of shear bands are seeded initially. Candidates include any residual heterogeneity left in the fluid by the initial procedure of sample preparation; imperfections in the alignment of the rheometer plates; true thermal noise with an amplitude set by  $k_B T$ ; and rheometer curvature in cone-and-plate or cylindrical Couette devices. We consider in particular the last of these because it is likely to be the dominant source of heterogeneity in commonly used flow cells, which typically have a curvature of about 10%.

While modeling the full effects of curvature is a complicated task, its dominant consequence can be captured simply by including a slight heterogeneity in the total stress field. (The assumption made above of a uniform stress across the gap only holds in an idealized planar device.) Accordingly, we set  $\Sigma(t) \rightarrow \Sigma(t)[1 + qh(y)]$  where  $q$  sets the amplitude of the curvature and  $h(y)$  is a function with an amplitude of  $O(1)$  that prescribes its spatial dependence. The detailed form of  $h(y)$  will differ from device to device: For example in a cylindrical Couette, it is known to have a  $1/r^2$  dependence, where  $r$  is the radial coordinate. However, the aim here is not to model any particular device geometry in detail, but simply to capture the dominant effect of curvature in seeding the flow heterogeneity. Accordingly, we set  $h(y) = \cos(\pi/L)$  which is the lowest Fourier mode to fit into the simulation cell while still obeying the boundary conditions at the walls.

#### IV. SHEAR BANDING IN OTHER TIME-DEPENDENT PROTOCOLS

As a preamble to presenting our results for shear banding in oscillatory flow protocols in Secs. V and VI, we first briefly collect together criteria derived in previous work for linear instability to the formation of shear bands in simpler time-dependent protocols: Slow shear rate sweep, fast shear startup, and step stress.

##### A. Slow shear rate sweep

A common experimental protocol consists of slowly sweeping the shear rate  $\dot{\gamma}$  upward (or downward) in order to measure a fluid's (quasi) steady state flow curve. In this protocol, the criterion for linear instability to the onset of shear banding, given a base state of initially homogeneous shear flow, has long been known to be [24]

$$\frac{\partial \Sigma}{\partial \dot{\gamma}} < 0. \quad (22)$$

##### B. Fast shear startup

Another common experimental protocol consists of taking a sample of fluid that is initially at rest and with any residual stresses well relaxed, then suddenly jumping the strain rate from zero to some constant value such that  $\dot{\gamma}(t) = \dot{\gamma}_0 \Theta(t)$ , where  $\Theta(t)$  is the Heaviside function. Commonly measured in response to this applied flow is the time-dependent stress signal  $\Sigma(t)$  as it evolves toward its eventual steady state value, for that particular applied shear rate, on the fluid's flow curve. This evolution typically has the form of an initial elastic regime with  $\Sigma \approx G\gamma$  while the strain  $\gamma$  remains small, followed by an overshoot in the stress at a strain of  $O(1)$ , then a decline to the final steady state stress on the flow curve. In [47,48,50], we gave evidence that the presence of an overshoot in this stress startup signal is generically indicative of a strong tendency to form shear bands, at least transiently. These bands may, or may not, then persist for as

long as the shear remains applied, according to whether or not the underlying constitutive curve of stress as a function of strain rate is nonmonotonic.

Such behavior is to be expected intuitively. Consider a shear startup run performed at a high enough strain rate that the material's response is initially elastic, with the stress startup signal depending only on the accumulated strain  $\gamma = \dot{\gamma}t$  and not separately on the strain rate  $\dot{\gamma}$ . The decline in stress following an overshoot in the stress startup signal corresponds to a negative derivative

$$\frac{\partial \Sigma}{\partial \gamma} < 0. \quad (23)$$

This clearly has the same form as Eq. (22) above, with the strain rate now replaced by the strain. As such it is the criterion that we might intuitively expect for the onset of strain bands in a nonlinear elastic solid, following the early intuition of [52].

In close analogy to this intuitive expectation, for a complex fluid subject to a fast, elastically dominated startup the criterion for the onset of banding was shown in [47] to be that the stress signal  $\Sigma(\gamma = \dot{\gamma}t)$  of the initially homogeneous startup flow obeys

$$-\text{tr} \mathbf{M} \frac{\partial \Sigma}{\partial \dot{\gamma}} + \dot{\gamma} \frac{\partial^2 \Sigma}{\partial \dot{\gamma}^2} < 0, \quad (24)$$

where  $\text{tr} \mathbf{M} < 0$  in this startup protocol. This result holds exactly for any model whose equations are of the generalized form in Sec. III above, and have only two relevant dynamical variables,  $d = 2$ . (Recall that for the nRP model these two variables are the shear stress  $W_{xy}$  and one component of normal stress  $W_{yy}$ , in units in which the polymer modulus  $G = 1$ .) The criterion (24) closely resembles the simpler form Eq. (23) motivated intuitively above, with an additional term informed by the curvature in the signal of stress as a function of strain. The effect of this additional term is to trigger the onset of banding just *before* overshoot, as the stress startup signal starts to curve downward from its initial regime of linear elastic response.

What this criterion tells us is that the presence of an overshoot in the stress signal of an underlying base state of initially homogeneous shear startup acts as a causative trigger for the formation of shear bands. A common misconception is that instead it is the onset of shear banding that causes the stress drop. While it is true that the onset of banding may reduce the stress further compared to that expected on the basis of a homogeneous calculation, we emphasize that the direction of mechanistic causality here is that the stress drop following overshoot causes shear banding and not (primarily) vice versa.

With criterion (24) in mind, theorists should be alert that any model predicting startup stress overshoot in a calculation in which the flow is artificially constrained to remain homogeneous is likely to further predict the formation of shear bands in a full heterogeneous calculation that allows bands to form. Likewise, experimentalists should be alert that any observations of stress overshoot in shear startup is strongly

suggestive of the presence of banding in the material's flow profile.

In [48], the analytically derived criterion (24) was confirmed numerically for fast shear startup in the nRP model, where it should indeed apply exactly due to the presence of just  $d=2$  relevant dynamical variables  $W_{xy}$  and  $W_{yy}$  in that model. It was also shown to apply to good approximation in the sRP model, for which  $d=3$ , for strain rates lower than the inverse stretch relaxation time (where the dynamics of the sRP model indeed well approximate those of the nRP model).

Banding associated with startup stress overshoot has also been demonstrated in several numerical studies of SGMs [3,49,51]. (The term SGM is used to describe a broad class of materials including foams, emulsions, colloids, surfactant onion phases, and microgels, all of which show structural disorder, metastability, a yield stress, and often also rheological ageing below the yield stress.) In these soft glasses, however, it should be noted that the decrease in stress following the startup overshoot arises from increasing plasticity rather than falling elasticity. This makes it more difficult to derive an analytical criterion analogous to Eq. (24). Accordingly, the theoretical evidence for shear banding following startup overshoot in these soft glasses, while very convincing, remains primarily numerical to date.

Consistent with these theoretical predictions, experimental observations of banding associated with startup stress overshoot are widespread: In wormlike micellar surfactants [41,44], polymers [14,16,33,34,36,55–57], carbopol gels [6,32], and Laponite clay suspensions [7]. Nonetheless, we also note other studies of polymer solutions [19] where stress overshoot is seen without observable banding. It would be particularly interesting to see further experimental work on polymeric fluids to delineate more fully the regimes, for example entanglement number and degree of polydispersity, in which banding arises with sufficient amplitude to be observed experimentally.

### C. Step stress

Besides the strain-controlled protocols just described, a fluid's rheological behavior can also be probed under conditions of imposed stress. In a step stress experiment, an initially well relaxed fluid is suddenly subject to the switch-on of a shear stress  $\Sigma_0$  that is held constant thereafter, such that  $\Sigma(t) = \Theta(t)\Sigma_0$ . Commonly measured in response to this applied stress is the material's creep curve,  $\gamma(t)$ , or the temporal derivative of this,  $\dot{\gamma}(t)$ . In [47], the criterion for linear instability to the formation of shear bands, starting from a state of initially homogeneous creep shear response, was shown to be that

$$\frac{\partial^2 \dot{\gamma}}{\partial t^2} / \frac{\partial \dot{\gamma}}{\partial t} > 0. \quad (25)$$

This tells us that shear banding should be expected in any step stress experiment in which the differentiated creep response curve simultaneously curves upward and slopes upward. (Indeed, it should also be expected in any experiment where

that response function simultaneously curves downward and slopes downward, though we do not know of any instances of such behavior.) This prediction has been confirmed numerically in the RP model of polymers and wormlike micelles [48], as well as in the soft glassy rheology model of foams, dense emulsions, microgels, etc [3].

Experimentally, shear banding associated with a simultaneously upwardly curving and upwardly sloping differentiated creep response curve has indeed been seen in entangled polymers [14,33,34,41,44–46,57], carbopol microgels [43], and carbon black suspensions [42].

## V. LARGE AMPLITUDE OSCILLATORY STRAIN

We now consider shear banding in the time-dependent strain-imposed oscillatory protocol of LAOStrain. Here a sample of fluid, initially well relaxed at time  $t=0$ , is subject for times  $t>0$  to a strain of the form

$$\gamma(t) = \gamma_0 \sin(\omega t), \quad (26)$$

to which corresponds the strain rate

$$\dot{\gamma}(t) = \gamma_0 \omega \cos(\omega t) = \dot{\gamma}_0 \cos(\omega t). \quad (27)$$

After an initial transient, once many cycles have been executed, the response of the system is expected to attain a state that is time-translationally invariant from cycle to cycle,  $t \rightarrow t + 2\pi/\omega$ . All the results presented below are in this long-time regime, usually for the  $N=20$ th cycle after the flow commenced. The dependence of the stress on the cycle number was carefully studied in wormlike micelles in [81].

To characterize any given applied LAOStrain, we must clearly specify two quantities: The strain amplitude and the frequency  $(\gamma_0, \omega)$ , or alternatively the strain rate amplitude and the frequency  $(\dot{\gamma}_0, \omega)$ , where  $\dot{\gamma}_0 = \gamma_0 \omega$ . In what follows we usually choose the latter pairing  $(\dot{\gamma}_0, \omega)$ . Any given LAOStrain experiment is then represented by its location in that plane of  $\dot{\gamma}_0$  and  $\omega$ . See Fig. 1.

In any experiment where the applied strain rate remains small,  $\dot{\gamma}_0 \ll 1$ , a regime of linear response is expected. (Recall that in dimensional form this condition corresponds to  $\dot{\gamma}_0 \tau_d \ll 1$ .) But even in an experiment where the strain rate does not remain small, linear response can nonetheless still be expected if the overall applied strain remains small,  $\gamma_0 \ll 1$ . Accordingly, linear response should obtain in the region below the long-dashed line marked in Fig. 1. Because shear banding is an inherently nonlinear phenomenon, we expect the interesting region of this  $(\dot{\gamma}_0, \omega)$  plane from our viewpoint to be in the nonlinear regime, above the long-dashed line, and we focus our attention mostly on this in what follows.

Besides considering whether any given applied LAOStrain will result in linear or nonlinear response, also relevant is the characteristic timescale  $1/\omega$  of the oscillation compared to the fluid's intrinsic terminal relaxation timescale  $\tau_d = 1$ . For low frequencies  $\omega \ll 1$ , to the left of the leftmost dotted line in Fig. 1, we expect the material's

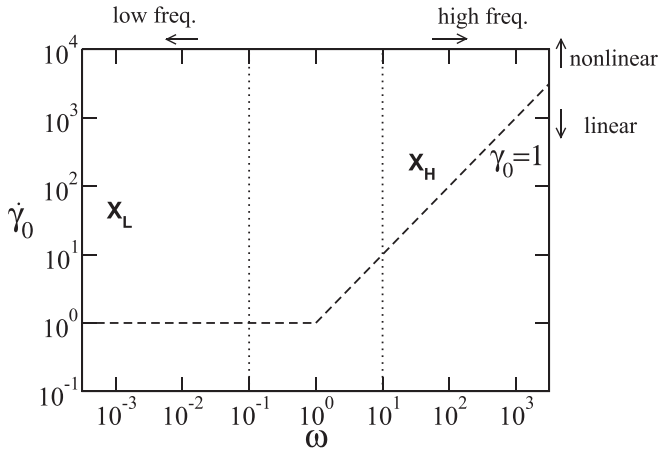


**FIG. 1.** LAOStrain: Sketch of regions of shear rate amplitude and frequency space in which we expect limiting low frequency viscous and high frequency elastic behaviors, and regimes of linear and nonlinear response. LAOStrain runs at the locations marked  $X_L$  and  $X_H$  are explored in Figs. 2 and 3 for the nRP model with nonmonotonic and monotonic underlying constitutive curve, respectively.

reconfiguration dynamics to keep pace with the applied deformation. This will lead to quasisteady state response in which the stress slowly sweeps up and down the steady state flow curve as the shear rate varies through a cycle. In contrast for high frequencies  $\omega \gg 1$ , to the right of the rightmost dotted line in Fig. 1, the material’s relaxation dynamics cannot keep pace with the applied deformation and we expect elasticlike response.

We illustrate these two limiting regimes by studying the response of the nRP model to an imposed LAOStrain at each of the two locations marked  $X_L$  and  $X_H$  in Fig. 1. For simplicity, for the moment, we artificially constrain the flow to remain homogeneous and confine ourselves to calculating the uniform base state as outlined in Sec. III A. The results are shown in Fig. 2 for the nRP model with parameters for which the underlying constitutive curve is nonmonotonic such that (in any heterogeneous calculation) the fluid would show shear banding under conditions of steady applied shear.

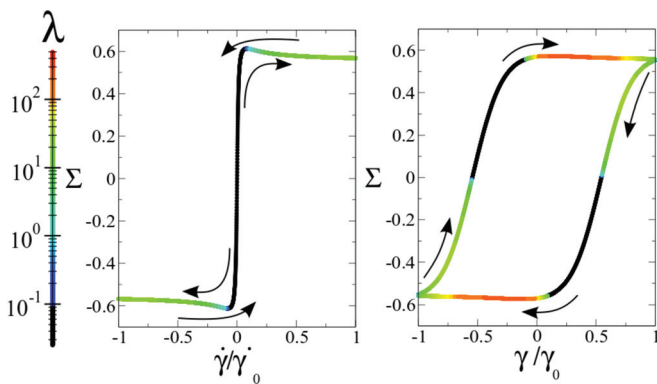


**FIG. 2.** LAOStrain in the nRP model with a nonmonotonic underlying constitutive curve. Model parameters  $\beta = 0.4$ ,  $\eta = 10^{-5}$ . Left: Viscous Lissajous–Bowditch figure shows stress  $\Sigma$  versus strain rate  $\dot{\gamma}$  for an imposed frequency and strain rate  $(\omega, \dot{\gamma}_0) = (0.001, 50.0)$  marked as  $X_L$  in the low frequency regime of Fig. 1. Right: Elastic Lissajous–Bowditch figure shows stress  $\Sigma$  versus strain  $\gamma$  for an imposed frequency and strain rate  $(\omega, \dot{\gamma}_0) = (31.6, 200.0)$  marked as  $X_H$  in the high frequency regime of Fig. 1. Color scale shows eigenvalue.

Figure 3 shows results with model parameters for which the constitutive curve is monotonic such that no banding would be expected in steady shear flow.

The left panels of Figs. 2 and 3 contain results for the low frequency oscillation marked  $X_L$  in Fig. 1. Here we choose to plot the stress response  $\Sigma(t)$  in a Lissajous–Bowditch figure as a parametric function of the time-varying imposed strain rate  $\dot{\gamma}(t)$ , consistent with the expectation of fluidlike response in this low-frequency regime. (Throughout the paper, we shall describe such a plot of stress versus strain rate as being in the “viscous” representation.) As can be seen, in each case the fluid indeed tracks up and down its (quasi) steady state homogeneous constitutive curve  $\Sigma(\dot{\gamma})$  in the range  $-\dot{\gamma}_0 < \dot{\gamma} < \dot{\gamma}_0$ . For any set of model parameters, several of these LAOStrain response curves  $\Sigma(\dot{\gamma})$  collected together for different  $\dot{\gamma}_0$  and low frequency  $\omega$  would all collapse onto this master constitutive curve.

Also shown by the color scale in the left panels of Figs. 2 and 3 is the eigenvalue as introduced in Sec. III B. Recall that a positive eigenvalue at any point in the cycle strongly suggests that the homogeneous base state is linearly unstable to the development of shear banding at that point in the cycle. (In any region where this scale shows black, the eigenvalue is either negative, or so weakly positive as to cause only negligible banding growth.) As expected, a regime of instability is indeed seen in Fig. 2, in the region where the constitutive curve has negative slope

$$\frac{\partial \Sigma}{\partial \dot{\gamma}} < 0. \quad (28)$$

For a fluid with a monotonic constitutive curve, no instability is observed at this low frequency (Fig. 3, left).

The corresponding results for the high frequency run marked  $X_H$  in Fig. 1 are shown in the right panels of Figs. 2 and 3. Here we choose to plot the stress response  $\Sigma(t)$  in a Lissajous–Bowditch figure as a parametric function of the time-varying strain  $\gamma(t)$ , in the so-called elastic representation. Indeed, just as in the low frequency regime, the material behaved as a viscous fluid with the stress response falling onto the steady state master constitutive curve in the viscous representation  $\Sigma(\dot{\gamma})$ , for a high frequency cycle we might instead expect a regime of elastic response in which only the

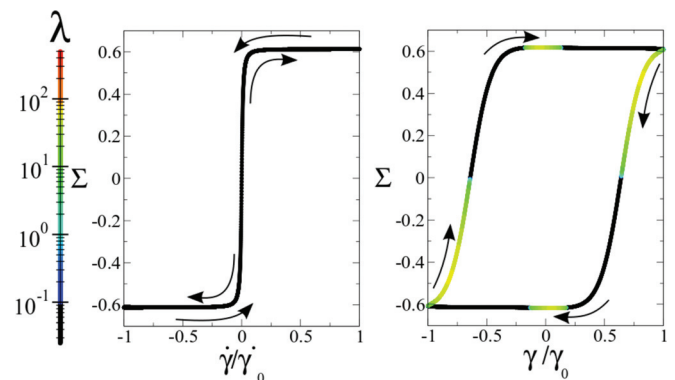


**FIG. 3.** As in Fig. 2, but for a value of the CCR parameter  $\beta = 1.0$ , for which the underlying homogeneous constitutive curve is monotonic.

accumulated strain is important, and not (separately) the strain rate, giving a master response curve of stress versus strain,  $\Sigma(\gamma)$ .

We might further have intuitively expected this curve to be the same as that obtained in a fast shear startup from rest, with (in the positive strain part of the cycle) elastic response  $\Sigma \approx G\gamma$  at low strain  $\gamma \ll 1$ , followed by stress overshoot at a typical strain  $\gamma = +O(1)$ , then decline toward a constant stress at larger strains (with the symmetric curve in the negative-strain part of the cycle such that  $\Sigma \rightarrow -\Sigma$  for  $\gamma \rightarrow -\gamma$ ). In other words, in LAOStrain at high frequency, we might have expected the system to continuously explore its elastic shear startup curve  $\Sigma(\gamma)$  between  $\gamma = -\gamma_0$  and  $\gamma = +\gamma_0$ .

However, this intuition is not met in a straightforward way. In the right panels of Figs. 2 and 3, we observe instead an open cycle that is explored in a clockwise sense as time proceeds through an oscillation: The stress transits the upper part of the loop (from bottom left to top right) in the forward part of the cycle as the strain increases from left to right, and the symmetry-related lower part of the loop in the backward part, where the strain decreases from right to left.

This can be understood as follows. For any LAOStrain run at high frequency  $\omega \gg 1$  but in the linear regime with strain amplitude  $\gamma_0 \ll 1$ , we do indeed find the stress response to fall onto a closed master curve  $\Sigma(\gamma)$ , which also corresponds to that obtained in a fast stress startup from rest, with linear elastic response  $\Sigma \approx G\gamma$ . (Data not shown.) In contrast, for amplitudes  $\gamma_0 > 1$ , the system only explores this startup-from-rest curve in the first half of the *first* cycle after the inception of flow. (This has the usual form, with elastic response for small strains, stress overshoot at a strain  $\gamma = O(1)$ , then decline to a constant stress.) In the second half of the cycle, when the strain rate reverses and the strain decreases, the stress response departs from the startup-from-rest curve. With hindsight this is in fact obvious: As this backward shear part of the cycle commences the initial condition is not that of a well-relaxed fluid, but one that has just suffered a large forward strain.

The same is true for the next forward half cycle: Its initial condition is that of a fluid that has just suffered a large negative strain, corresponding to the lower left point in the right panel of Figs. 2 or 3. Starting from that initial condition, the stress evolution nonetheless thereafter resembles that of a fast startup, with an initial fast rise followed by an overshoot then decline to constant stress, before doing the same in reverse (with a symmetry-related “negative overshoot”) during the next half cycle, giving the open curves as described. Associated with this overshoot in each half cycle is a positive eigenvalue indicating instability to the onset of shear banding. Importantly, we note that this arises even in the case of a monotonic underlying constitutive curve (Fig. 3, right), and therefore even in a fluid that would not display steady state banding under a steadily applied shear flow. It is the counterpart for LAOStrain of the elastic banding triggered by stress overshoot in a fast shear startup from rest, as explored previously in [47,48,50].

Indeed, following the calculation first set out in [47], it is straightforward to show that the condition for a linear

instability to banding in this elastic high frequency regime  $\omega \gg 1$  is the same as in fast shear startup

$$-\text{tr}\mathbf{M} \frac{\partial \Sigma}{\partial \gamma} + \dot{\gamma} \frac{\partial^2 \Sigma}{\partial \gamma^2} < 0. \quad (29)$$

As already discussed, this gives a window of instability setting in just before the stress overshoot (or negative overshoot) in each half cycle in the right panels of Fig. 2 and 3 due to (in the positive  $\dot{\gamma}$  part of the cycle in which the stress transits from bottom left to top right) the negatively sloping and curving  $\Sigma(\gamma)$ . An analogous statement applies in the other part of the cycle, with the appropriate sign reversals. Note that these overshoots are sufficiently weak as to be difficult to resolve by eye on the scale of Figs. 2 and 3.

Interestingly, Eq. (29) also predicts a region of (weaker) instability immediately after the reversal of strain in each half cycle, as also seen in the right panels of Figs. 2 and 3. Analytical considerations show that this additional regime of instability is not driven by any negative slope or curvature in  $\Sigma(\gamma)$ , but instead arises from a change in sign of  $\mathbf{M}$ . This instability has no counterpart that we know of in shear startup. Its associated eigenvector is dominated by the normal stress component  $W_{yy}$ , rather than the strain rate or shear stress. Heterogeneity in this quantity could feasibly be accessed in birefringence experiments.

The results of Figs. 2 and 3 can be summarized as follows. At low frequencies, the system sweeps slowly up and down the underlying constitutive curve  $\Sigma(\dot{\gamma})$  as the shear rate varies through the cycle. If that curve is nonmonotonic, this homogeneous base state is unstable to shear banding in the region of negative constitutive slope,  $d\Sigma/d\dot{\gamma} < 0$ . At high frequencies, the system instead executes a process reminiscent of elastic shear startup in each half cycle, but with an initial condition corresponding to the state left by the shear of opposite sense in the previous half cycle. Associated with this is a stress overshoot in each half cycle, giving instability to elastic shear banding. Crucially, this elastic instability occurs whether or not the underlying constitutive curve is nonmonotonic or monotonic, and therefore whether or not the fluid would shear band in steady shear.

From a practical experimental viewpoint, it is important to note that, whereas in a single shear startup run these elastic strain bands would form transiently then heal back to homogeneous flow (unless the sample has a nonmonotonic underlying constitutive curve and so also bands in steady state), in LAOStrain the banding will recur in each half cycle and so be potentially easier to access experimentally. Any time-averaging measurement should of course only take data in the forward part of each cycle, to avoid averaging to zero over the cycle.

Having explored in Figs. 2 and 3, the tendency to form shear bands in two particular LAOStrain runs (one in the limit of low frequency,  $X_L$  in Fig. 1, and one in the limit of high frequency,  $X_H$ ), we now explore the full  $(\dot{\gamma}_0, \omega)$  plane of Fig. 1 by showing in Figs. 4 and 5 color maps of the extent of shear banding across this plane. Recall that each pinpoint in this plane corresponds to a single LAOS experiment with strain rate amplitude  $\dot{\gamma}_0$  and frequency  $\omega$ . To build up these

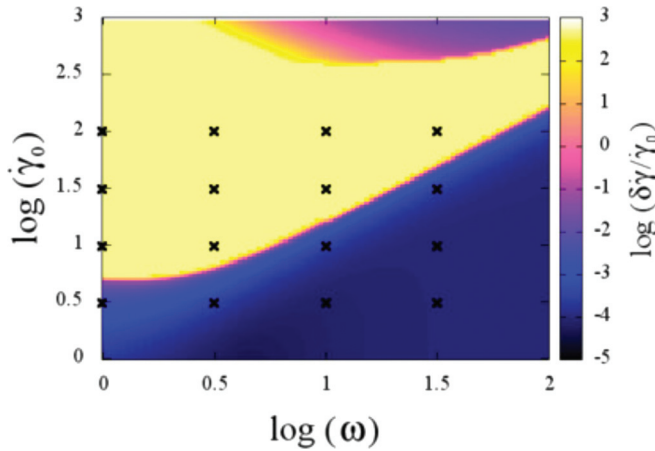


**FIG. 4.** Color map of the normalized degree of shear banding for the nRP model with a nonmonotonic constitutive curve. Each point in this  $\dot{\gamma}_0, \omega$  plane corresponds to a particular LAOStrain run with strain rate amplitude  $\dot{\gamma}_0$  and frequency  $\omega$ . For computational efficiency, these calculations are performed by integrating the linearized equations in Sec. III B. Reported is the maximum degree of banding that occurs at any point in the cycle, after many cycles. Model parameters:  $\beta = 0.4$ ,  $\eta = 10^{-5}$ . Cell curvature  $q = 10^{-4}$ . Crosses indicate the grid of values of  $\dot{\gamma}_0$  and  $\omega$  in Pipkin diagram of Fig. 6.

color maps, we sweep over a grid of  $100 \times 100$  values of  $\dot{\gamma}_0, \omega$  and execute a LAOStrain run at each point. Solving the model's full nonlinear dynamics on such a dense grid would be unfeasibly time-consuming computationally. Therefore at each  $\dot{\gamma}_0, \omega$  we instead integrate the linearized equations set out in Sec. III B. In each such run, we record the degree of banding  $\delta\dot{\gamma}$ , maximized over the cycle after many cycles. It is this quantity, normalized by the maximum strain rate amplitude  $\dot{\gamma}_0$ , that is represented by the color scale in Figs. 4 and 5.

Figure 4 pertains to the nRP model with model parameters for which the underlying constitutive curve is nonmonotonic. As expected, significant banding (bright/yellow region) is observed even in the limit of low frequency  $\omega \rightarrow 0$  for strain rate amplitudes  $\dot{\gamma}_0$  exceeding the onset of negative slope in the underlying constitutive curve. This region of banding is the direct (and relatively trivial) analog of banding in a slow strain rate sweep along the steady state flow curve.

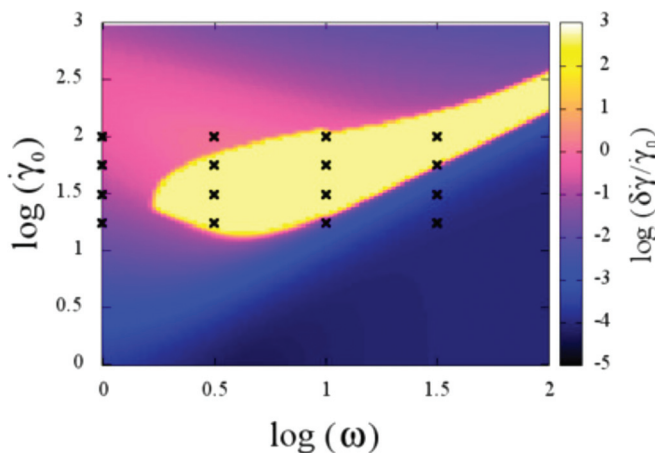


**FIG. 5.** As in Fig. 4, but with a CCR parameter  $\beta = 1.0$ , for which the fluid has a monotonic underlying constitutive curve. Crosses indicate the grid of values of  $\dot{\gamma}_0$  and  $\omega$  used in the Pipkin diagram of Fig. 7.

Figure 5 shows results for the nRP model with parameters such that the underlying constitutive curve is monotonic. Here steady state banding is absent in the limit  $\omega \rightarrow 0$ . In both Figs. 4 and 5, however, significant banding is observed at high frequencies for a strain amplitude  $\dot{\gamma}_0 > 1$ : This is the elastic banding associated with the stress overshoot in each half cycle, described in detail above for the  $(\dot{\gamma}_0, \omega)$  values denoted by  $X_H$  in Fig. 1.

It is important to emphasize, therefore, that even a fluid with a purely monotonic constitutive curve, which does not shear band in steady flow, is still nonetheless capable of showing strong shear banding in a time-dependent protocol of high enough frequency (Fig. 5). Also important to note is that for a fluid with a nonmonotonic constitutive curve, the region of steady state viscous banding at low frequencies crosses over smoothly to that of elastic banding as the frequency increases (Fig. 4).

Corresponding to the degree of banding in the shear rate  $\delta\dot{\gamma}$ , as plotted in Figs. 4 and 5, is an equivalent degree of banding  $G\delta W_{xy} = -\eta\delta\dot{\gamma}$  (to within small corrections of order the cell curvature,  $q$ ) in the shear component of the polymeric conformation tensor. This follows trivially by imposing force balance at zero Reynolds number. Counterpart maps for the degree of banding in the component  $\delta W_{yy}$  of the polymeric conformation tensor can also be built up. These reveal closely similar regions of banding to those shown in Figs. 4 and 5. (Data not shown.) Experimentally, heterogeneities in the polymeric conformation tensor can be accessed by flow birefringence.

As noted above, to build up such comprehensive roadmaps as in Figs. 4 and 5 in a computationally efficient way, we omitted all nonlinear effects and integrated instead the linearized equations of Sec. III B. These are only strictly valid in any regime where the amplitude of the heterogeneity remains small. In omitting nonlinear effects, they tend to overestimate the degree of banding in any regime of sustained positive eigenvalue, in predicting the heterogeneity to grow exponentially without bound, whereas in practice it would be cut off by nonlinear effects. We now remedy this shortcoming by exploring the model's full nonlinear spatio-temporal dynamics. To do so within feasible computational run times, we focus on a restricted grid of values in the  $\dot{\gamma}_0, \omega$  plane, marked by crosses in Figs. 4 and 5.

The results are shown in Fig. 6 for the nRP model with model parameters for which the underlying constitutive curve is nonmonotonic. At low frequencies, the results tend toward the limiting fluidlike behavior discussed above, in which the stress slowly tracks up and down the steady state flow curve  $\Sigma(\dot{\gamma})$  (Progression toward this limit can be seen by following the top row of panels in Fig. 6(b) to the left.). Viscous banding is seen for sufficiently high strain rate amplitudes  $\dot{\gamma}_0$  due to the negatively sloping underlying homogeneous constitutive curve. At high frequencies, the response tends instead toward the limiting elasticlike behavior discussed above. For large enough strain amplitudes, the stress then shows an open cycle  $\Sigma(\dot{\gamma})$  as a function of strain, with an overshoot in each half cycle that triggers the formation of elastic banding. [Progression toward this limit is seen by following the top row of panels in Fig. 6(a) to the right.]

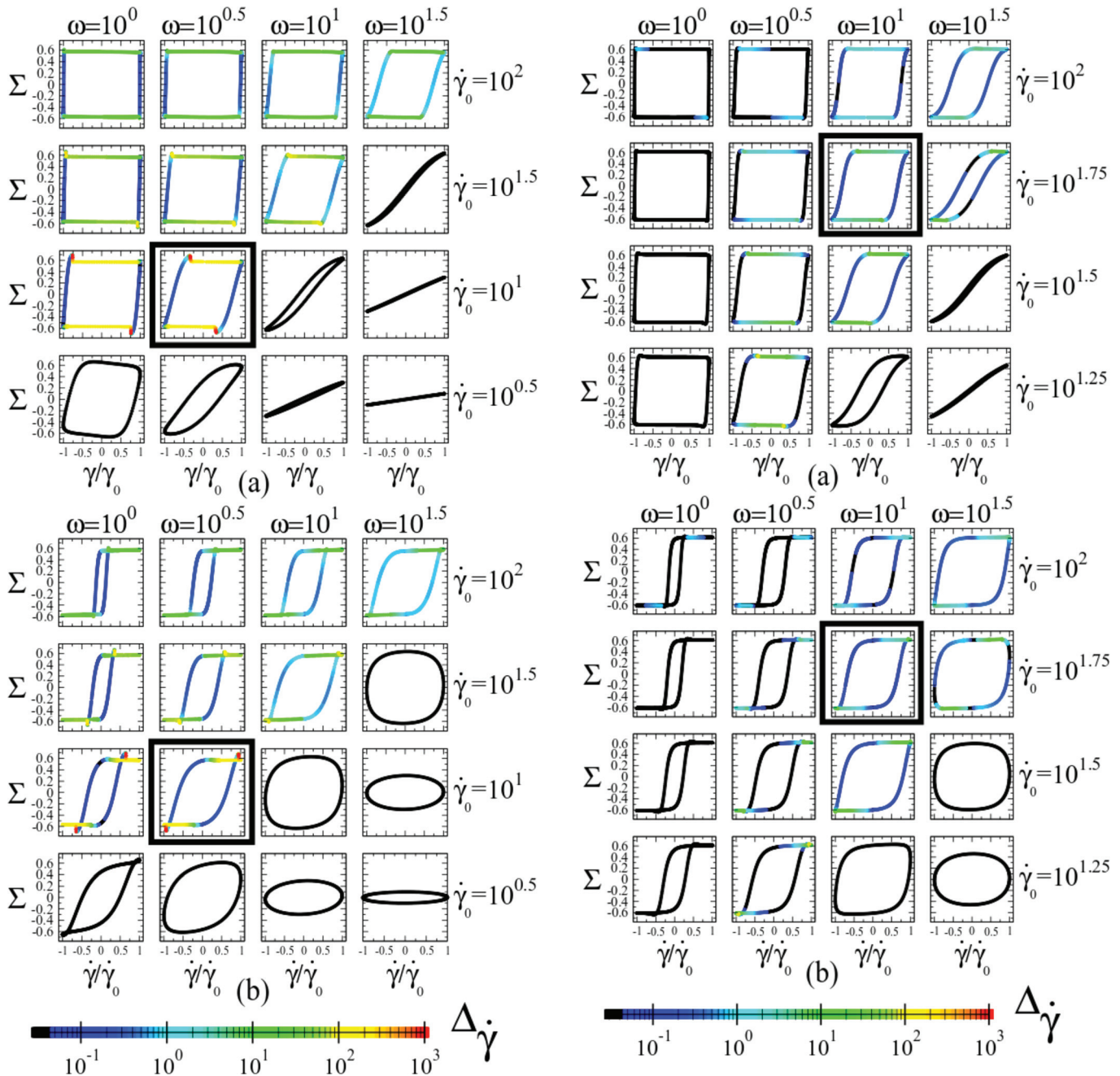


**FIG. 6.** Lissajous–Bowditch curves in LAOstrain for the nRP model with a nonmonotonic constitutive curve. Results are shown in the elastic representation in (a), and the viscous representation in (b). Columns of fixed frequency  $\omega$  and rows of fixed strain-rate amplitude  $\dot{\gamma}_0$  are labeled at the top and right-hand side. Color scale shows the time-dependent degree of shear banding. Model parameters:  $\beta = 0.4, \eta = 10^{-5}$ . Cell curvature:  $q = 10^{-4}$ . Number of numerical grid points  $J = 512$ . A detailed portrait of the run outlined by the thicker box is shown in Fig. 8.

Overshoots in the elastic Lissajous–Bowditch curve of stress as a function of strain have been identified in earlier work [82] as leading to self-intersection of the corresponding viscous Lissajous–Bowditch curve of stress as a function of strain rate. Such an effect is clearly seen here in the RP model: See for example the runs highlighted by the thicker boxes in Figs. 6 and 7.

For intermediate frequencies, the stress is a complicated function of both strain rate and also, separately, the strain.

**FIG. 7.** As in Fig. 6 but for a value of the CCR parameter  $\beta = 1.0$ , for which the fluid’s underlying constitutive curve is monotonic. Number of numerical grid points  $J = 512$ . A detailed portrait of the run outlined by the thicker box is shown in Fig. 9.

The three dimensional curve  $(\Sigma, \dot{\gamma}, \gamma)$  is then best shown as two separate projections: First in the elastic representation of the  $\Sigma, \gamma$  plane [Fig. 6(a)], and second, in the viscous representation of the  $(\Sigma, \dot{\gamma})$  plane [Fig. 6(b)]. Collections of these Lissajous–Bowditch curves on a grid of  $(\dot{\gamma}_0, \omega)$  values as in Fig. 6 are called Pipkin diagrams.

For the particular LAOstrain run highlighted by a thicker box in Fig. 6, a detailed portrait of the system’s dynamics is shown in Fig. 8. Here the stress is shown in the elastic representation, as a function of strain  $\gamma$  (left hand panel). Two curves are shown here. The first shows the stress signal in a calculation in which the flow is artificially constrained to remain homogeneous. A linear instability analysis for the

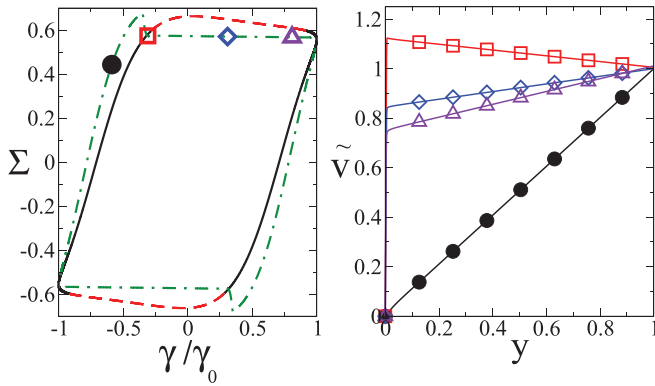


**FIG. 8.** LAOstrain in the nRP model with a nonmonotonic constitutive curve. Strain rate amplitude  $\dot{\gamma}_0 = 10.0$  and frequency  $\omega = 3.16$ . Model parameters  $\beta = 0.4, \eta = 10^{-5}$ . Cell curvature  $q = 10^{-4}$ . Number of numerical grid points  $J = 1024$ . Left: Stress response in the elastic representation. Solid black and red-dashed line: Calculation in which the flow is constrained to be homogeneous. Red-dashed region indicates a positive eigenvalue showing instability to the onset of shear banding. Green dot-dashed line: Stress response in a full nonlinear simulation that allows banding. Right: Velocity profiles corresponding to stages in the cycle indicated by matching symbols in the left panel. Each profile is normalized by the speed of the moving plate.

dynamics of small heterogeneous perturbations about this time-evolving homogeneous base state then reveals instability toward the formation of shear bands (a positive eigenvalue) in the portion of that curve shown as a red dashed line. A full nonlinear simulation then reveals the formation of shear bands and leads to a stress signal (green dot-dashed line) that deviates from that of the homogeneously constrained calculation, in particular in having a much more precipitous stress drop due to the formation of bands.

The associated velocity profiles at four points round the part of the cycle with increasing strain are shown in the right panel. Before the stress overshoot, no banding is apparent (black circles). The overshoot then triggers strong shear banding (red squares), with most of the shear concentrated in a thin band at the left hand edge of the cell. Interestingly, the shear in the right hand part of the cell is in the opposite sense to the overall applied shear. This is consistent with the fact that the stress is a decreasing function of strain in this regime: The material is being unloaded, and an elasticlike material being unloaded will shear backward. As the overall

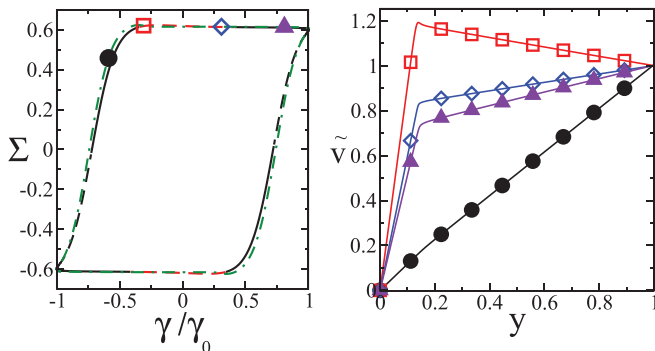


**FIG. 9.** As in Fig. 8 but for the nRP model with a CCR parameter  $\beta = 1.0$  for which the underlying homogeneous constitutive curve is monotonic, and for a LAOstrain with strain rate amplitude  $\dot{\gamma}_0 = 56.2$  and frequency  $\omega = 10.0$ . Number of numerical grid points  $J = 512$ .

applied strain increases toward the end of the window of instability, the flow heterogeneity gradually decays away. This process repeats in each half cycle (with the obvious sign reversals in the part of the cycle in which the strain is decreasing).

The corresponding Pipkin diagram for a fluid with a monotonic constitutive curve (Fig. 7) likewise confirms its counterpart linear diagram in Fig. 5. Here viscous banding is absent at low frequencies because the fluid is not capable of steady state banding. Crucially, however, a strong effect of elastic banding is still seen at high frequencies. A detailed portrait of the system’s dynamics in this elastic regime, for the strain rate amplitude and frequency marked by the thicker box in Fig. 7, is shown in Fig. 9. As can be seen, it shows similar features to those just described in Fig. 8. We emphasize, then, that even polymeric fluids that do not band under conditions of steady shear are still capable of showing strong banding in a time-dependent protocol at high enough frequency. This important prediction is consistent with the early insight of Adams and Olmsted in [73].

So far, we have presented results for the nRP model, which assumes an infinitely fast rate of chain stretch relaxation compared to the rate of reptation such that the ratio  $\tau_R/\tau_d \rightarrow 0$ . This corresponds to assuming that the polymer chains are very highly entangled, with a number of entanglements per chain  $Z = \tau_d/3\tau_R \rightarrow \infty$ . We now consider the robustness of these results to reduced entanglement numbers, and accordingly increased chain stretch relaxation time  $\tau$  (in units of  $\tau_d$ ).

The results are summarized in Fig. 10, which shows the regions of the plane of the CCR parameter  $\beta$  and entanglement number  $Z$  in which significant banding (filled circles), observable banding (hatched circles), and no banding (open circles) occur. (Recall that results presented for the nRP

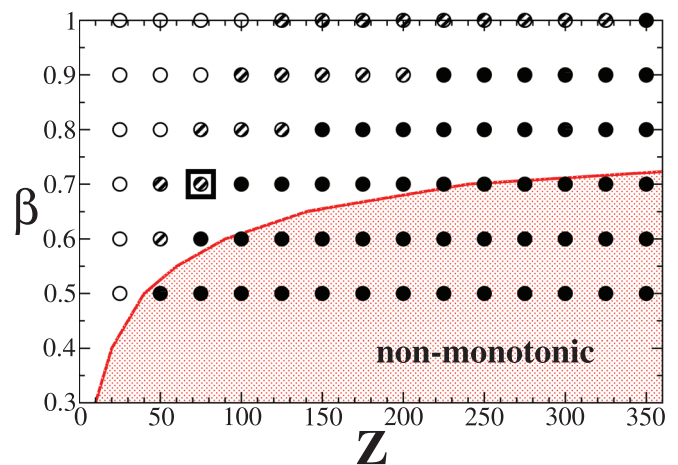


**FIG. 10.** Effect of CCR parameter  $\beta$  and entanglement number  $Z$  (and so of chain stretch relaxation time  $\tau_R = \tau_d/3Z$ ) on shear banding in LAOstrain. (Recall that the nonstretching version of the model has  $\tau_R \rightarrow 0$  and so  $Z \rightarrow \infty$ .) Empty circles: No observable banding. Hatched circles: Observable banding, typically  $\Delta\dot{\gamma}/\dot{\gamma}_0 \approx 10\%–100\%$ . Filled circles: Significant banding  $\Delta\dot{\gamma}/\dot{\gamma}_0 \geq 100\%$ . For hatched and filled symbols we used the criterion that banding of the typical magnitude stated is apparent in a region spanning at least half a decade by half a decade in the plane of  $\dot{\gamma}_0, \omega$ , by examining maps as in Fig. 11 in by eye. The square shows the parameter values explored in detail in Fig. 11.

model above pertain to the values  $\beta = 0.4, 1.0$  in the limit  $Z \rightarrow \infty$ .) As can be seen, by reducing the number of entanglements per chain, the effect of shear banding is reduced and eventually eliminated. However it is important to note that, depending on the value of  $\beta$ , significant banding is still observed for experimentally commonly used entanglement numbers, typically in the range 20 – 100. Furthermore, significant banding is seen in a large region of the  $(\beta, Z)$  plane for which the material's underlying constitutive curve is monotonic. As discussed above, there is no current consensus as to the value of the CCR parameter  $\beta$  in the range  $0 < \beta < 1$ . Using the route map provided in Fig. 10, a study of shear banding in LAOStrain experiments could provide one way to obtain a more accurate estimate of the value of this parameter.

For the pairing of  $\beta$  and  $Z$  values marked by the square in Fig. 10, we show in Fig. 11 a color map of the degree of banding expected in LAOStrain in the space of strain rate amplitude  $\dot{\gamma}_0$  and frequency  $\omega$ . This figure, which is for the sRP model, is the counterpart of the earlier Figs. 4 and 5 discussed above for the nRP model, with the degree of banding calculated for computational efficiency within the assumption of linearized dynamics. Recall that each pinpoint in this plane corresponds to a single LAOStrain run with applied strain rate  $\dot{\gamma}(t) = \dot{\gamma}_0 \cos(\omega t)$ .

Consistent with the underlying constitutive curve being monotonic for these parameters, viscous banding is absent in the limit of low frequencies  $\omega \rightarrow 0$ . However, significant banding is still observed for runs with strain rate amplitudes  $O(10\text{--}100)$  and frequencies  $O(1\text{--}10)$ . This is the counterpart of the elastic banding reported above in the nRP model, though the effect of finite chain stretch in the sRP model is to moderate the degree of banding. A detailed portrait of the model's nonlinear banding dynamics at a strain rate amplitude  $\dot{\gamma}_0$  and frequency  $\omega$  marked by the cross in Fig. 11 is

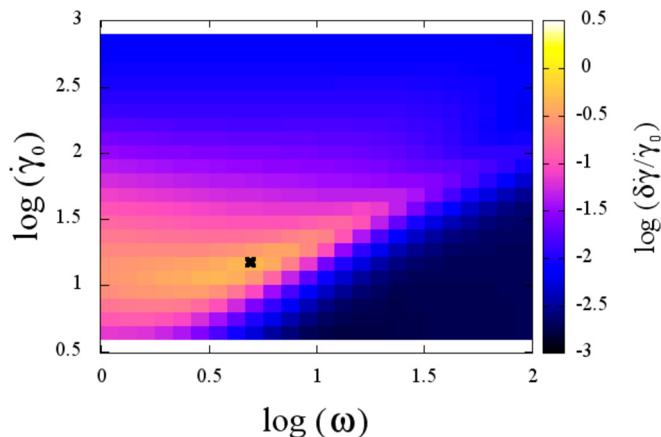


**FIG. 11.** Color map of the normalized degree of shear banding for the sRP model with a monotonic constitutive curve. Each point in this  $\dot{\gamma}_0, \omega$  plane corresponds to a particular LAOStrain run with strain rate amplitude  $\dot{\gamma}_0$  and frequency  $\omega$ . For computational efficiency, these calculations are performed by integrating the linearized equations in Sec. III B. Reported is the maximum degree of banding at any point in the cycle, after many cycles. Model parameters:  $\beta = 0.7, Z = 75$  (and so  $\tau_R = 0.0044$ ),  $\eta = 10^{-5}$ . Cell curvature  $q = 2 \times 10^{-3}$ . Note the different color scale from Figs. 2 and 3. The model's full nonlinear dynamics for the  $(\dot{\gamma}_0, \omega)$  value marked by the cross are explored in Fig. 12.

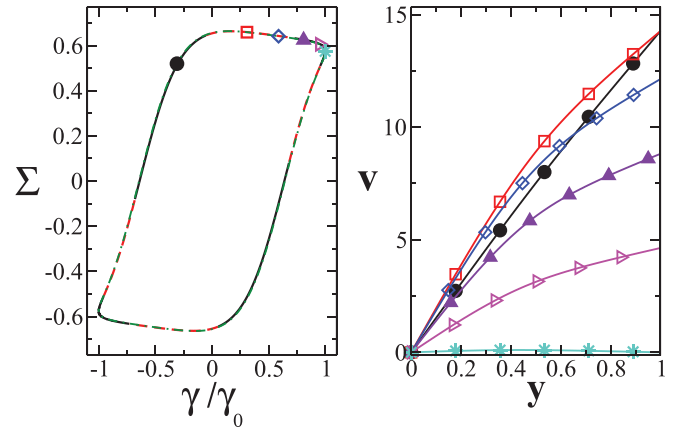


**FIG. 12.** sRP model with a monotonic constitutive curve in LAOStrain of strain rate amplitude  $\dot{\gamma}_0 = 20.0$  and frequency  $\omega = 8.0$ . Model parameters  $\beta = 0.7, Z = 75, \eta = 10^{-5}$ . Cell curvature  $q = 2 \times 10^{-3}$ . Number of numerical grid points  $J = 512$ . Left: Stress response in the elastic representation. Solid black and red-dashed line: Calculation in which the flow is constrained to be homogeneous. Red-dashed region indicates a positive eigenvalue showing instability to the onset of shear banding. Green dot-dashed line: Stress response in a full nonlinear simulation that allows banding (almost indistinguishable from homogeneous signal in this case). Right: Velocity profiles corresponding to stages in the cycle indicated by matching symbols in left panel.

shown in Fig. 12. Significant shear banding associated with the stress overshoot is apparent in each half cycle.

## VI. LARGE AMPLITUDE OSCILLATORY STRESS

We now consider the time-dependent stress-imposed oscillatory protocol of LAOStress. Here the sample is subject for times  $t > 0$  to a stress of the form

$$\Sigma(t) = \Sigma_0 \sin(\omega t), \quad (30)$$

characterized by the frequency  $\omega$  and stress amplitude  $\Sigma_0$ . As for the case of LAOStrain above, all the results presented below are in the long-time regime, once many ( $N = 20$ ) cycles have been executed and the response of the system has settled to be time-translationally invariant from cycle to cycle,  $t \rightarrow t + 2\pi/\omega$ .

In Sec. IV C, we reviewed existing work demonstrating the tendency to form shear bands in a step stress experiment. Here an initially well relaxed sample is suddenly subject at time  $t = 0$  to the switch-on of a shear stress of amplitude  $\Sigma_0$ , which is held constant for all subsequent times. The criterion for an underlying base state of initially homogeneous creep response to become linearly unstable to the formation of shear bands is then that the time-differentiated creep response curve  $\dot{\gamma}(t)$  obeys [47]

$$\frac{\partial^2 \dot{\gamma}}{\partial t^2} / \frac{\partial \dot{\gamma}}{\partial t} > 0. \quad (31)$$

Therefore, shear banding is expected in any regime where the time-differentiated creep curve simultaneously slopes up and curves upward; or instead simultaneously slopes down and curves downward.

Having been derived within the assumption of an imposed stress that is constant in time, criterion (31) would not *a priori* be expected to hold for the case of LAOStress. Nonetheless, it might reasonably be expected to apply, to good approximation, in any regime of a LAOStress experiment where a separation of timescales arises such that the shear rate  $\dot{\gamma}(t)$  evolves on a much shorter timescale than the stress. In this case, from the viewpoint of the strain rate signal, the stress appears constant in comparison and the constant-stress criterion (31) is expected to hold. Indeed, in what follows we shall show that many of our results for LAOStress can be understood on the basis of this simple piece of intuition.

We start in Fig. 13 by considering the nRP model in a parameter regime for which the underlying constitutive curve is nonmonotonic (see the dotted line in the left panel) such that shear banding would be expected under conditions of a steadily applied shear rate. With the backdrop of this constitutive curve, we consider a LAOStress run at low frequency  $\omega \rightarrow 0$ . For definiteness, we will focus on the part of the cycle where the stress is positive, but analogous remarks will apply to the other half of the cycle, with appropriate changes of sign.

Consider first the regime in which the stress is slowly increased from 0 toward its maximum value  $\Sigma_0$ . In this part of the cycle, at the low frequencies of interest here, we expect the system to initially follow the high viscosity branch of the constitutive curve. In any experiment for which the final stress  $\Sigma_0$  exceeds the local maximum in the constitutive curve, the system must at some stage during this increasing stress part of the cycle transit from the high to low viscosity branch of the constitutive curve. This transition is indeed seen in Fig. 13: It occurs via “top jumping” from the stress maximum across to the low viscosity branch. Conversely, on the downward part of the sweep as the stress decreases from its maximum value  $\Sigma_0$ , the system initially follows the low viscosity branch until it eventually jumps back to the high viscosity branch. (We return in our concluding remarks to discuss the possible effect of thermal nucleation events, which are not included in these simulations, on

this process of jumping between the two branches of the constitutive curve.)

The corresponding signal of strain rate versus time during this slow up-then-down stress oscillation is shown in the right panel of Fig. 13. As can be seen, the regimes where the shear rate transits between the two different branches of the constitutive curve occur over relatively short time intervals. (The duration of this process is informed by the short timescale  $\eta/G$ , whereas the stress evolves on the much longer timescale  $2\pi/\omega$ .) This separation of timescales renders the stress signal approximately constant in comparison to the fast evolution of the strain rate. Criterion (31) might therefore be expected to apply in this regime of transition, at least to good approximation.

Furthermore, during the transition from the high to low viscosity branch, we see a regime in which the shear rate signal simultaneously slopes up and curves up as a function of time: Criterion (31) not only applies but is also met, and we therefore expect an instability to banding. Plotting, by means of a color scale, the eigenvalue as defined in Sec. III B, we find that it is indeed positive. Likewise, during the rapid transition back from the low to high viscosity branch, we find a regime in which the shear rate signal simultaneously slopes down and curves down. As seen from the color scale, the eigenvalue is also positive in this regime (although more weakly than during the upward transition). In what follows, we will confirm the expectation of shear band formation during these times of positive eigenvalue by simulating the model’s full nonlinear spatiotemporal dynamics.

These processes of rapid transition between different branches of the constitutive curve are of course not expected in a LAOStress experiment at low frequency for a fluid with a monotonic constitutive curve. In this case, for a LAOStress run in the limit  $\omega \rightarrow 0$  the system instead sweeps quasistatically along the monotonic constitutive curve, with no associated banding. As in the case of LAOStrain, however, it is crucial to realise that the absence of banding in an experiment at zero frequency does not preclude the possibility of banding in a time-dependent protocol at finite frequency, even in a fluid with a monotonic constitutive curve.

With this in mind, we show in Fig. 14 the counterpart of Fig. 13, but now for the nRP model with a monotonic

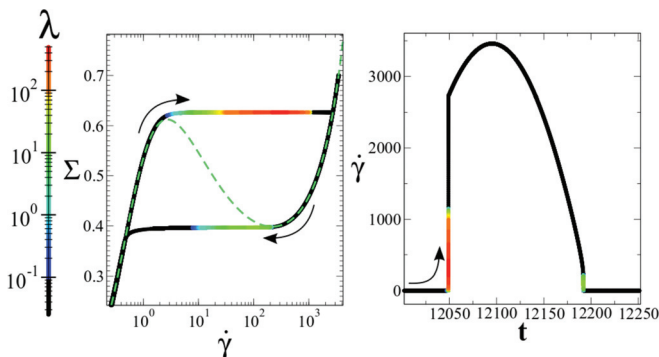


**FIG. 13.** LAOStress in the nRP model with a nonmonotonic constitutive curve. Model parameters:  $\beta = 0.1$ ,  $\eta = 10^{-4}$ . Frequency  $\omega = 0.01$  and stress amplitude  $\Sigma_0 = 0.7$ . Left: Stress versus strain rate (shown on a log scale) in the positive stress part of the cycle. Color scale shows eigenvalue, with negative values also shown as black. Green dashed line: Underlying constitutive curve. Right: Corresponding stress versus time plot.

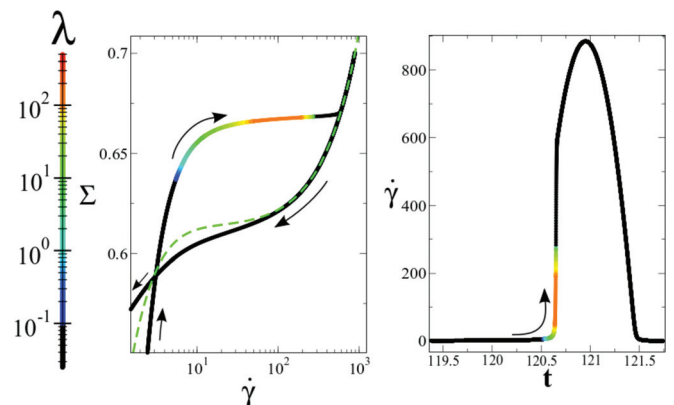


**FIG. 14.** As in Fig. 13 but at a higher imposed frequency  $\omega = 1.0$  and for a value of the CCR  $\beta = 0.9$ , for which the nRP model has a monotonic underlying constitutive curve. Right: Corresponding stress versus time plot.

constitutive curve subject to a LAOStress run at a finite frequency  $\omega = 1$ , of order the fluid's reciprocal stress relaxation timescale. The key to understanding the emergent dynamics in this case is the existence in the underlying zero-frequency constitutive curve (shown by a dotted line in the left panel) of a region in which the stress is a relatively flat (though still increasing) function of the strain rate. As the system transits this region during the increasing stress part of a finite-frequency stress cycle, we again observe a regime of quite sudden progression from low to high strain rate. This is seen in the left to right transition in the stress versus strain rate representation in the left panel of Fig. 14, and (correspondingly) in the rapid increase of strain rate versus time in the right panel.

During this regime of rapid transit, we again have conditions in which the strain rate evolves rapidly compared to the stress such that the constant-stress criterion (31) should apply to good approximation. Furthermore, during the first part of the transition, the strain rate signal simultaneously slopes and curves upward as a function of time. The eigenvalue is therefore positive, indicating linear instability of an initially homogeneous base state to the formation of shear bands. We will again confirm this prediction by simulating the model's full nonlinear spatiotemporal dynamics below.

In the context of Figs. 13 and 14, we have discussed the dynamics of the nRP model with a nonmonotonic and monotonic constitutive curve, respectively, focusing in each case on one particular value of the imposed frequency  $\omega$  and stress amplitude  $\Sigma_0$ . We now consider the full plane of  $(\Sigma_0, \omega)$  by showing in Figs. 15 and 16 color maps of the extent of banding across it. Recall that each point in this plane corresponds to a single LAOS experiment with stress amplitude  $\Sigma_0$  and frequency  $\omega$ . To build up these maps, we sweep over a grid of  $20 \times 20$  values of  $\Sigma_0, \omega$  and execute at each point a LAOStress run, integrating the model's linearized equations set out in Sec. III B. We then represent the

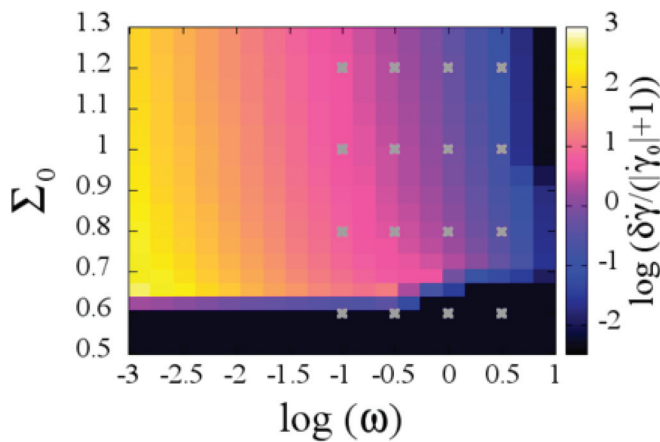


**FIG. 15.** Color map of the normalized degree of shear banding for the nRP model with a nonmonotonic constitutive curve. Each point in this  $\Sigma_0, \omega$  plane corresponds to a particular LAOStress run with stress amplitude  $\Sigma_0$  and frequency  $\omega$ . For computational efficiency, these calculations are performed by integrating the linearized equations in Sec. III B. Reported is the maximum degree of banding that occurs at any point in the cycle, after many cycles. Model parameters:  $\beta = 0.4$ ,  $\eta = 10^{-4}$ . Cell curvature  $q = 2 \times 10^{-3}$ . Crosses indicate the grid of values of  $\Sigma_0$  and  $\omega$  in Fig. 17.

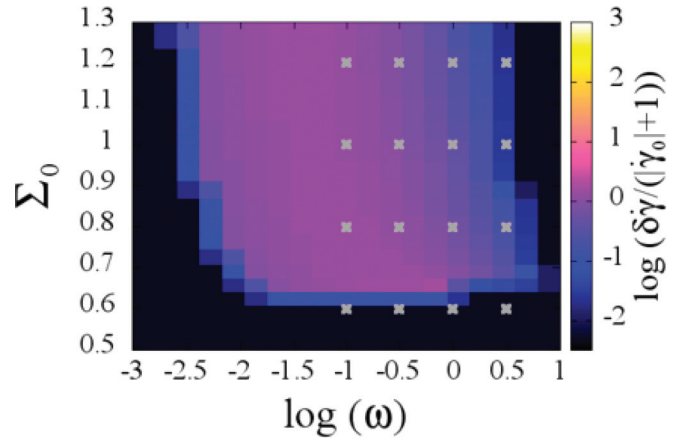


**FIG. 16.** As in Fig. 4, but with a CCR parameter  $\beta = 0.9$ , for which the fluid has a monotonic underlying constitutive curve. Crosses indicate the grid of values of  $\Sigma_0$  and  $\omega$  used in the Pipkin diagram of Fig. 18.

degree of banding  $\delta\dot{\gamma}$ , maximized over the cycle after many cycles, by the color scale.

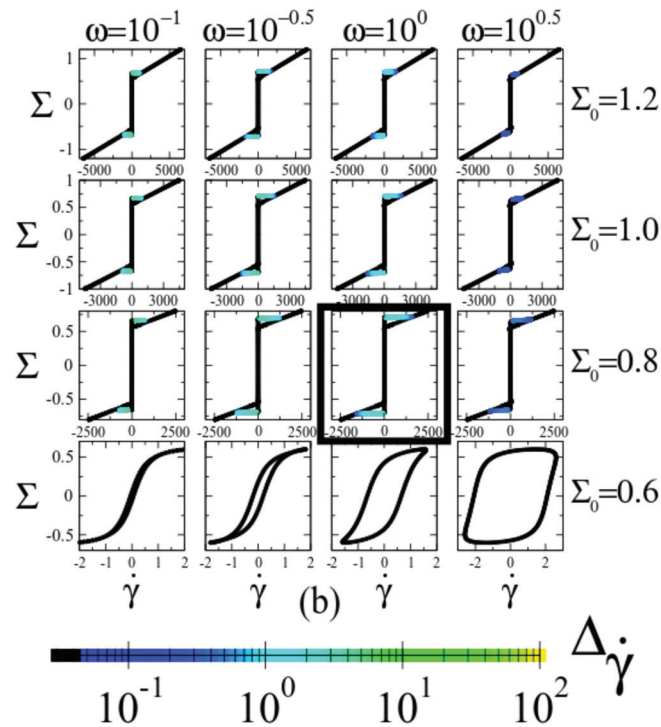
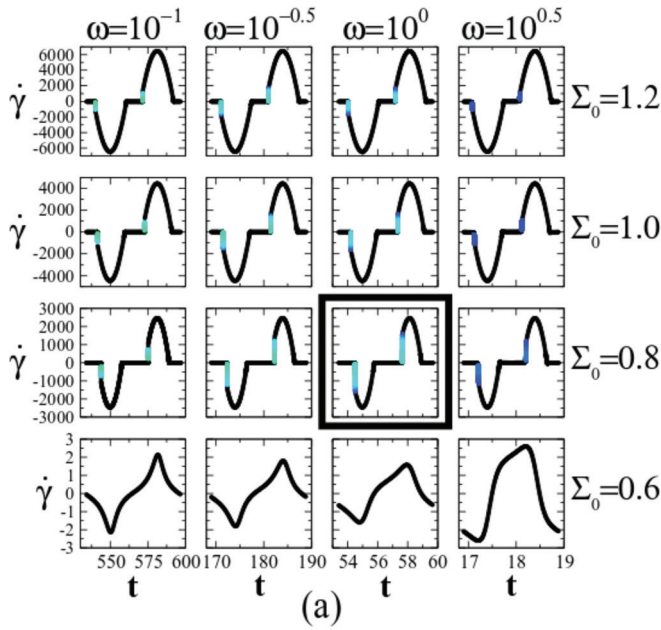
Figure 15 shows results with model parameters for which the underlying constitutive curve is nonmonotonic. As expected, for stress amplitudes  $\Sigma_0$  exceeding the local maximum in the underlying constitutive curve, significant banding is observed even in the limit of low frequency  $\omega \rightarrow 0$ . This is associated with the processes of jumping between the two different branches of the constitutive curve discussed above.

Figure 16 shows results for the nRP model with a monotonic underlying constitutive curve. Here steady state banding is absent in the limit  $\omega \rightarrow 0$ , as expected. However, significant banding is still nonetheless observed at frequencies of order the reciprocal reptation time, for imposed stress amplitudes exceeding the region of weak slope in the constitutive curve, consistent with our discussion of Fig. 14 above.

To obtain the comprehensive roadmaps of Figs. 15 and 16 in a computationally efficient way, we discarded any nonlinear effects and integrated the linearized model equations set out in Sec. III B. However, these linearized equations tend to overestimate the degree of banding in any regime of sustained positive eigenvalue. Therefore in Figs. 17 and 18, we now simulate the model's full nonlinear spatiotemporal dynamics, restricting ourselves for computational efficiency to grids of  $4 \times 4$  values of  $\Sigma_0, \omega$  as marked by crosses in Figs. 15 and 16.

Figure 17 pertains to the nRP model with model parameters for which the underlying constitutive curve is nonmonotonic. At low frequencies, the results tend toward the limiting behavior discussed above, in which the stress slowly tracks up and down the steady state flow curve  $\Sigma(\dot{\gamma})$  in between regimes of sudden transition between the two branches of the curve, during which shear bands form. This is most pronounced in the case of the jump between the high and low viscosity branches during the upward sweep. Banding on the downward sweep is only apparent in a relatively more limited region of  $\Sigma_0, \dot{\gamma}$  space, consistent with the transition of  $\dot{\gamma}_0$  being more modest in this part of the cycle during which the stress decreases.

For the particular run highlighted by the thicker box in Fig. 17, a detailed portrait of the system's dynamics is shown



**FIG. 17.** Lissajous–Bowditch curves in LAOStress for the nRP model with a nonmonotonic constitutive curve. Results are shown as shear-rate versus time in (a), and in the viscous representation of stress versus strain rate in (b). Columns of fixed frequency  $\omega$  and rows of fixed strain-rate amplitude  $\dot{\gamma}_0$  are labeled at the top and right-hand side. Color scale shows the time-dependent degree of shear banding. Model parameters:  $\beta = 0.4, \eta = 10^{-4}, l = 0.02$ . Cell curvature:  $q = 2 \times 10^{-3}$ . Number of numerical grid points  $J = 512$ . A detailed portrait of the run outlined by the thicker box is shown in Fig. 19.

in Fig. 19. The left panel shows the strain rate signal as a function of time, zoomed on the region in which the strain rate makes its transit from the high to low viscosity branch of the constitutive curve. The black and red-dashed lines show the results of a calculation in which the flow is artificially constrained to remain homogeneous. The red-dashed region indicates the regime in which the criterion (31) for

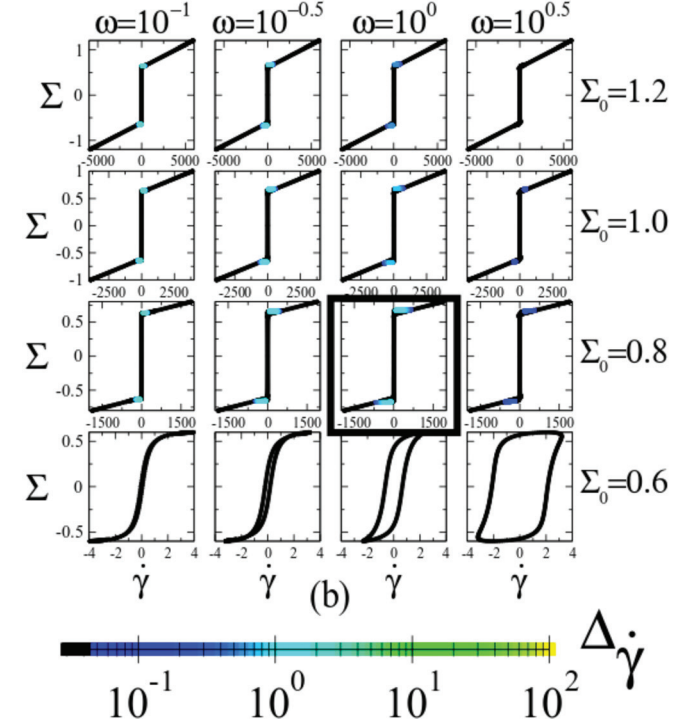
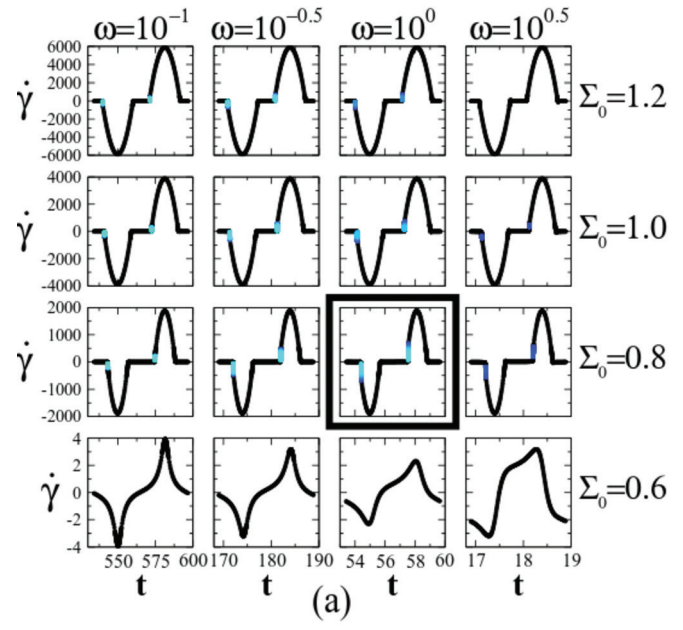


**FIG. 18.** As in Fig. 17 but for a value of the CCR parameter  $\beta = 0.9$ , for which the fluid’s underlying constitutive curve is monotonic. Number of numerical grid points  $J = 512$ . A detailed portrait of the run outlined by the thicker box is shown in Fig. 20.

linear instability to the formation of shear bands is met, which also corresponds to the regime in which the strain rate signal simultaneously slopes up and curves upward.

In a simulation that properly takes account of flow heterogeneity, shear bands indeed develop during this regime where the criterion is met, then decay again once the strain rate signal curves down and stability is restored. This sequence can be seen in the velocity profiles in the right hand panel. The stress signal associated with this run that allows bands to form is shown by the green dot-dashed line in the left panel, and is only barely distinguishable from that

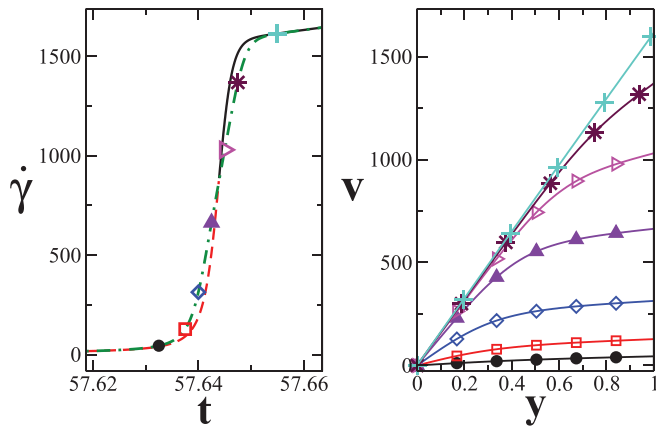


**FIG. 19.** LAOStress in the nRP model with a nonmonotonic constitutive curve. Stress amplitude  $\Sigma_0 = 0.8$  and frequency  $\omega = 1.0$ . Model parameters  $\beta = 0.4, \eta = 10^{-4}, l = 0.02$ . Cell curvature  $q = 2 \times 10^{-3}$ . Number of numerical grid points  $J = 512$ . Left: Strain rate response as a function of time, focusing on the region in which the system transits from the high to low viscosity branch of the constitutive curve. Solid black and red-dashed line: Calculation in which the flow is constrained to be homogeneous. Red-dashed region indicates a positive eigenvalue showing instability to the onset of shear banding. Green dot-dashed line: Stress response in a full nonlinear simulation that allows banding. Right: Velocity profiles corresponding to stages in the cycle indicated by matching symbols in the left panel.

of the run in which the flow is constrained to remain homogeneous.

Figure 18 pertains to the nRP model with model parameters for which the underlying constitutive curve is monotonic, with the grid of  $(\Sigma_0, \omega)$  values that it explores marked by crosses in Fig. 16. True top-jumping events are absent here, and no shear banding arises in the limit of zero frequency. As discussed above, however, a similar rapid transition from low to high shear rate is seen in runs at a frequency  $O(1)$ , as the stress transits the region of weak slope in the constitutive curve during the increasing stress part of the cycle. Associated with this transit is a pronounced tendency to form shear bands.

This can be seen for the run highlighted by the thicker box in Fig. 18, of which a detailed portrait is shown in Fig. 20. This shows very similar features to its counterpart for a non-monotonic underlying constitutive curve. In particular, the

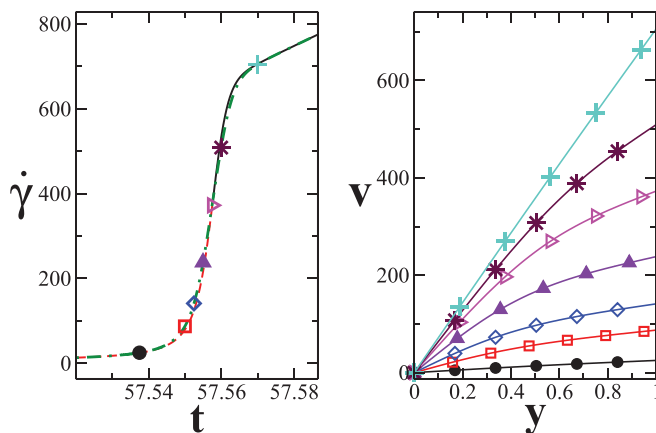


**FIG. 20.** As in Fig. 19 but for the nRP model with a CCR parameter  $\beta = 0.9$  for which the underlying homogeneous constitutive curve is monotonic. Number of numerical grid points  $J = 512$ .

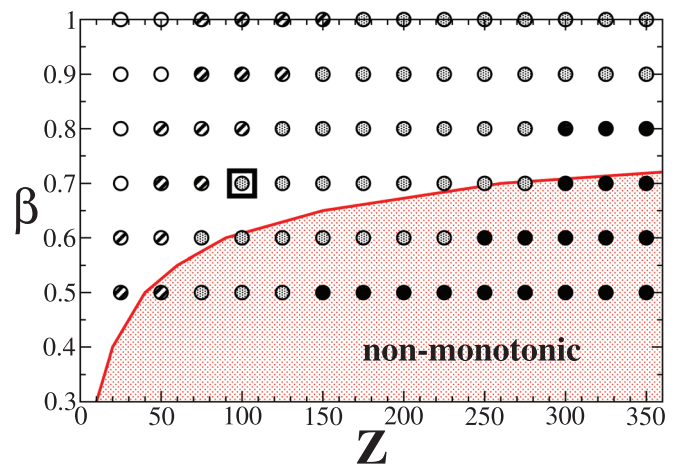
regime of simultaneous upward slope and upward curvature in the strain rate signal as the stress transits the region of weak positive constitutive slope triggers pronounced shear banding.

These results illustrate again the crucial point: That shear bands can form in a protocol with sufficiently strong time dependence, even in a fluid for which the underlying constitutive curve is monotonic such that banding is forbidden in steady state flows.

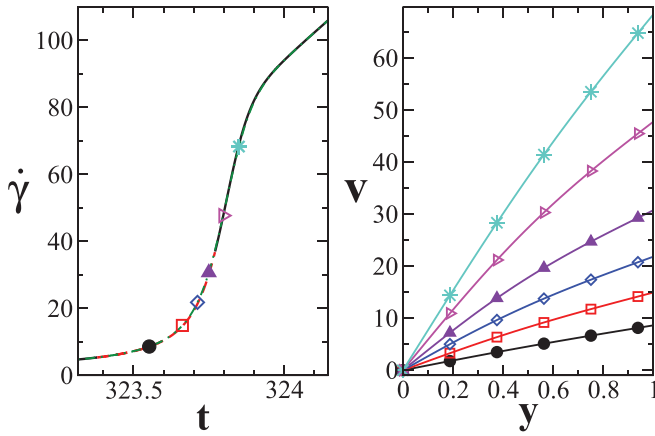
So far, we have restricted our discussion of LAOStress to the nRP model, for which the stretch relaxation time  $\tau_r$  is set to zero upfront so that any chain stretch relaxes to zero instantaneously, however strong the applied flow. The results of these calculations are expected to apply, to good approximation, to experiments performed in flow regimes where chain stretch remains small. This typically imposes the restriction  $\dot{\gamma}\tau_R \ll 1$ . We now turn to the sRP model to consider the effects of finite chain stretch in experiments where this restriction is not met.

Figure 21 shows the regions of the plane of the CCR parameter  $\beta$  and entanglement number  $Z$  in which banding can be expected even with chain stretch. As for the case of LAOStrain above we note that, depending on the value of  $\beta$ , significant banding is still observed for experimentally commonly used entanglement numbers, typically in the range 20–100. Furthermore, observable banding is clearly evident over a large region of this plane in which the underlying constitutive curve is monotonic, precluding steady state banding. Again, we hope that this figure might act as a roadmap to inform the discussion concerning the value of the CCR parameter  $\beta$ .

For the pairing of  $\beta$  and  $Z$  values marked by the square in Fig. 21, we show in Fig. 22 a detailed portrait of the model's



**FIG. 21.** Effect of CCR parameter  $\beta$  and entanglement number  $Z$  (and so of chain stretch relaxation time  $\tau_R = \tau_d/3Z$ ) on shear banding in LAOStress. (Recall that the nonstretching version of the model has  $\tau_R \rightarrow 0$  and so  $Z \rightarrow \infty$ .) Empty circles: No observable banding. Hatched circles: Observable banding,  $\Delta_{\dot{\gamma}}/(1 + |\dot{\gamma}(t)|) = 10\%–31.6\%$ . Dot-filled circles: Significant banding,  $\Delta_{\dot{\gamma}}/(1 + |\dot{\gamma}(t)|) = 31.6\%–100\%$ . Filled circles: Strong banding,  $\Delta_{\dot{\gamma}}/(1 + |\dot{\gamma}(t)|) > 100\%$ . For the hatched, dot-filled, and filled symbols, we used the criterion that banding of the typical magnitude stated is apparent for any of  $\omega = 0.1, 0.316$  or  $1.0$ , given a stress amplitude  $\Sigma_0$  exceeding the region of weak slope in the constitutive curve. The square shows the parameter values explored in detail in Fig. 22. The solvent viscosity  $\eta$  is  $3.16 \times 10^{-5}$ .



**FIG. 22.** sRP model with a monotonic constitutive curve in LAOStress of stress amplitude  $\Sigma_0 = 0.8$  and frequency  $\omega = 0.1$ . Model parameters  $\beta = 0.7, Z = 100, \eta = 3.16 \times 10^{-5}$ . Cell curvature  $q = 2 \times 10^{-3}$ . Number of numerical grid points  $J = 512$ . Left: Strain rate signal versus time. Solid black and red-dashed line: Calculation in which the flow is constrained to be homogeneous. Red-dashed region indicates a positive eigenvalue showing instability to the onset of shear banding. Green dot-dashed line: Stress response in a full nonlinear simulation that allows banding (indistinguishable from homogeneous signal in this case.) Right: Velocity profiles corresponding to stages in the cycle indicated by matching symbols in left panel.

nonlinear dynamics at a stress amplitude  $\Sigma_0$  and frequency  $\omega$  for which observable banding occurs.

## VII. CONCLUSIONS

We have studied theoretically the formation of shear bands in LAOS in the RP model of polymers and wormlike micellar surfactants, with the particular aim of identifying the regimes of parameter space in which shear banding is significant, and the mechanisms that trigger its onset.

At low frequencies, the protocol of LAOStrain effectively corresponds to a repeating series of quasistatic sweeps up and down the steady state flow curve. Here, as expected, we see shear banding in those regimes of parameter space for which the fluid's underlying constitutive curve is nonmonotonic, for strain rate amplitudes large enough to enter the banding regime in which the stress is a characteristically flat function of strain rate.

In LAOStrain at higher frequencies, we report banding not only in the case of a nonmonotonic constitutive curve, but also over a large region of parameter space for which the constitutive curve is monotonic and so precludes steady state banding. We emphasize that this is an intrinsically time-dependent banding phenomenon that would be absent under steady state conditions, and we interpret it as the counterpart of the elastic banding predicted recently in the context of shear startup experiments at high strain rates [47].

In LAOStress, we report shear banding in those regimes of parameter space for which the underlying constitutive curve is either negatively or weakly positively sloping. In this case, the bands form during the process of yielding associated with the dramatic increase in shear rate that arises during that part of the cycle in which the stress magnitude transits the regime of weak constitutive slope in an upward direction. Although the banding that we observe here is

dramatically apparent during those yielding events, these events are nonetheless confined to a relatively small part of the stress cycle as a whole and would therefore need careful focus to be resolved experimentally. (A possible related protocol, more focused on the banding regime, could be to perform a shifted stress oscillation  $\Sigma(t) = \Sigma_{\text{plat}} + \Delta\Sigma \sin(\omega t)$  where  $\Sigma_{\text{plat}}$  is a characteristic stress value in the region of weak slope in the constitutive curve and  $\Delta\Sigma$  smaller in comparison.)

The dramatic increase in strain rate associated with transiting to the high shear branch in LAOStress is likely to present practical experimental difficulties in open flow cells such as Couette or cone-and-plate. To circumvent this, flow in a closed microfluidic channel provides an attractive alternative to those macroscopic geometries in seeking to access this effect experimentally.

In each case, we have demonstrated that the onset of shear banding can, for the most part, be understood on the basis of previously derived criteria for banding in simpler time-dependent protocols [47]. In particular, the trigger for banding in LAOStrain at low frequencies is that of a negatively sloping stress versus strain rate, which has long been recognized as the criterion for banding under conditions of a steady applied shear flow. The trigger in LAOStrain at high frequencies is instead that of an overshoot in the signal of stress as a function of strain, in close analogy to the criterion for banding onset during a fast shear startup run. The trigger for banding in LAOStress is that of a regime of simultaneous upward slope and upward curvature in the time-differentiated creep response curve of strain rate as a function of time. This again is a close counterpart to the criterion for banding following the imposition of a step stress.

For both LAOStrain and LAOStress, we have provided a map of shear banding intensity in the space of entanglement number  $Z$  and CCR parameter  $\beta$ . We hope that this will provide a helpful roadmap to experimentalists and might even help to pin down the value of the CCR parameter, for which no consensus currently exists.

We have also commented that the value of the Newtonian viscosity  $\eta$  is typically much smaller than the zero shear viscosity  $G\tau$  of the viscoelastic contribution, giving  $\eta \ll 1$  in our units. Experimental literature suggests a range  $\eta = 10^{-7}$ – $10^{-3}$ . We have typically used  $\eta = 10^{-5}$  or  $\eta = 10^{-4}$  in our numerics, and noted that the degree of banding tends to increase with decreasing  $\eta$ . We also noted that the timescale to transit from the high to low viscosity branch during yielding in each half cycle in LAOStress decreases with decreasing  $\eta/G$ . In view of these facts, a study of time-dependent banding in fluids with smaller values of  $\eta$  than those used here might warrant the inclusion of inertia because the small timescale for the propagation of momentum might exceed the short timescale  $\eta/G$  in those cases.

In all our numerical studies, the initial seed triggering the formation of shear bands was taken to be the weak curvature that is present in commonly used experimental flow cells. In order to demonstrate the principle that the banding we report requires only a minimal seed, rather than being an artefact of strong cell curvature, all our runs have assumed a curvature that is much smaller than that of most flow cells in practice.

We also neglected stochastic noise altogether in all the results presented here. (We have nonetheless also performed runs with small stochastic noise instead of cell curvature and find qualitatively all the same effects.)

However, one obvious shortcoming to this approach of taking only a very small initial seed is that it tends to suppress the nucleation events that are, in a real experimental situation, likely to trigger banding even before the regime of true linear instability [83], particularly in low frequency runs. It would therefore be interesting in future work to study the effect of a finite temperature with particular regard to the nucleation kinetics to which it would give rise.

The calculations performed in this work all assumed from the outset that spatial structure develops only in the flow gradient direction, imposing upfront translational invariance in the flow and vorticity directions. We defer to future work a study of whether, besides the basic shear banding instabilities predicted here, secondary instabilities [84] of the interface between the bands [85,86] or of the high shear band itself [87] will have time to form in any given regime of amplitude and frequency space.

We have ignored throughout the effects of spatial variations in the concentration field. However, it is well known that in a viscoelastic solution heterogeneities in the flow field, and in particular in the normal stresses, can couple to the dynamics of concentration fluctuations via a positive feedback mechanism that enhances the tendency to form shear bands [21,88–91]. In the calculations performed here in LAOS, we have observed significant differences in the viscoelastic normal stresses between the bands (approaching 50%–70% of the cycle-averaged value of the same quantity, at least in the calculations without chain stretch). It would therefore clearly be interesting in future work to consider the effects of concentration coupling on the phenomena reported here.

Throughout we have ignored the possibility of edge fracture because the one-dimensional calculations performed here lack any free surfaces and are unable to address it. It would clearly be interesting in future work to address the effects of edge fracture with regard to the phenomena considered here [17,19,92].

All the calculations performed here have adopted what is essentially a single-mode approach, taking account of just one reptation relaxation timescale  $\tau_d$  and one stretch relaxation timescale  $\tau_R$ . It would be interesting in future work to consider the effect of multiple relaxation timescales, which is likely to be an important feature of the dynamics of unbreakable polymers. (In wormlike micelles, in contrast, chain breakage and recombination narrows the relaxation spectrum significantly such that the single-mode approach adopted here is already likely to provide a reasonably full picture.)

We hope that this work will stimulate further experimental studies of shear banding in time-dependent flows of complex fluids, with a particular focus on the concept that banding is likely to arise rather generically during yielding-like events (following a stress overshoot in strain controlled protocols, or during a sudden increase in strain rate in stress-controlled protocols) even in fluids with a monotonic

constitutive curve that precludes steady state banding in a continuously applied shear. In polymers, this could form part of the lively ongoing debate concerning the presence or otherwise of shear banding in those materials. In wormlike micelles, it would be interesting to see a study of LAOS across the full phase diagram (as set out, for example, in [93]), from samples that band in steady state to those above the dynamical critical point, which do not.

## ACKNOWLEDGMENTS

The authors thank Alexei Likhtman, Elliot Marsden, Peter Olmsted, Rangarajan Radhakrishnan, Daniel Read, and Dimitris Vlassopoulos for interesting discussions. The research leading to these results has received funding from the European Research Council under the European Union's Seventh Framework Program (FP/2007-2013), ERC Grant Agreement No. 279365.

## References

- [1] Olmsted, P. D., "Perspectives on shear banding in complex fluids," *Rheol. Acta* **47**(3), 283–300 (2008).
- [2] Manneville, S., "Recent experimental probes of shear banding," *Rheol. Acta* **47**(3), 301–318 (2008).
- [3] Fielding, S. M., "Shear banding in soft glassy materials," *Rep. Prog. Phys.* **77**(10), 102601 (2014).
- [4] Divoux, T., M. A. Fardin, S. Manneville, and S. Lerouge, "Shear banding of complex fluids," *Annu. Rev. Fluid Mech.* **48**(1), 81–103 (2015).
- [5] Britton, M. M., and P. T. Callaghan, "Two-phase shear band structures at uniform stress," *Phys. Rev. Lett.* **78**(26), 4930–4933 (1997).
- [6] Divoux, T., D. Tamarii, C. Barentin, and S. Manneville, "Transient shear banding in a simple yield stress fluid," *Phys. Rev. Lett.* **104**(20), 208301 (2010).
- [7] Martin, J. D., and Y. Thomas Hu, "Transient and steady-state shear banding in aging soft glassy materials," *Soft Matter* **8**(26), 6940–6949 (2012).
- [8] Coussot, P., J. Raynaud, F. Bertrand, P. Moucheront, J. Guilbaud, H. T. Huynh, S. Jarny, and D. Lesueur, "Coexistence of liquid and solid phases in flowing soft-glassy materials," *Phys. Rev. Lett.* **88**(21), 218301 (2002).
- [9] Rodts, S., J. C. Baudez, and P. Coussot, "From "discrete" to "continuum" flow in foams," *Europhys. Lett.* **69**(4), 636–642 (2005).
- [10] Salmon, J.-B., S. Manneville, and A. Colin, "Shear banding in a lyotropic lamellar phase. I. Time-averaged velocity profiles," *Phys. Rev. E* **68**, 051503 (2003).
- [11] Berret, J.-F., and Y. S  r  ro, "Evidence of shear-induced fluid fracture in telechelic polymer networks," *Phys. Rev. Lett.* **87**, 048303 (2001).
- [12] Manneville, S., A. Colin, G. Waton, and F. Schosseler, "Wall slip, shear banding, and instability in the flow of a triblock copolymer micellar solution," *Phys. Rev. E* **75**, 061502 (2007).
- [13] Rogers, S. A., D. Vlassopoulos, and P. Callaghan, "Aging, yielding, and shear banding in soft colloidal glasses," *Phys. Rev. Lett.* **100**(12), 128304 (2008).
- [14] Tapadia, P., and S.-Q. Wang, "Yieldlike constitutive transition in shear flow of entangled polymeric fluids," *Phys. Rev. Lett.* **91**(19), 198301 (2003).
- [15] Tapadia, P., S. Ravindranath, and S.-Q. Wang, "Banding in entangled polymer fluids under oscillatory shearing," *Phys. Rev. Lett.* **96**(19), 196001 (2006).

- [16] Ravindranath, S., S.-Q. Wang, M. Olechnowicz, and R. P. Quirk, "Banding in simple steady shear of entangled polymer solutions," *Macromolecules* **41**(7), 2663–2670 (2008).
- [17] Li, Y., M. Hu, G. B. McKenna, C. J. Dimitriou, G. H. McKinley, R. M. Mick, D. C. Venerus, and L. A. Archer, "Flow field visualization of entangled polybutadiene solutions under nonlinear viscoelastic flow conditions," *J. Rheol.* **57**(5), 1411–1428 (2013).
- [18] Wang, S.-Q., G. Liu, S. Cheng, P. E. Boukany, Y. Wang, and X. Li, "Letter to the Editor: Sufficiently entangled polymers do show shear strain localization at high enough Weissenberg numbers," *J. Rheol.* **58**(4), 1059–1069 (2014).
- [19] Li, Y., and G. B. McKenna, "Startup shear of a highly entangled polystyrene solution deep into the nonlinear viscoelastic regime," *Rheol. Acta* **54**(9–10), 771–777 (2015).
- [20] Wang, S.-Q., S. Ravindranath, and P. E. Boukany, "Homogeneous shear, wall slip, and shear banding of entangled polymeric liquids in simple-shear rheometry: A roadmap of nonlinear rheology," *Macromolecules* **44**(2), 183–190 (2011).
- [21] Fielding, S. M., and P. D. Olmsted, "Flow phase diagrams for concentration-coupled shear banding," *Soft Matter* **11**(1), 65–83 (2003).
- [22] Doi, M., and S. F. Edwards, *The Theory of Polymer Dynamics* (Clarendon, Oxford, 1989).
- [23] Cates, M. E., "Nonlinear viscoelasticity of wormlike micelles (and other reversibly breakable polymers)," *J. Phys. Chem.* **94**(1), 371–375 (1990).
- [24] Yerushalmi, J., S. Katz, and R. Shinnar, "The stability of steady shear flows of some viscoelastic fluids," *Chem. Eng. Sci.* **25**(12), 1891–1902 (1970).
- [25] Cates, M. E., and S. M. Fielding, "Theoretical rheology of giant micelles," in *Giant Micelles*, edited by R. Zana and E. Kaler (Taylor and Francis, London, 2007), Chap. 4, pp. 109–161.
- [26] Berret, J.-F., "Rheology of wormlike micelles: Equilibrium properties and shear banding transitions," in *Molecular Gels*, edited by R. G. Weiss and P. Terech (Springer, Dordrecht, 2005), Chap. 19, pp. 667–720.
- [27] Snijkers, F., R. Pasquino, P. D. Olmsted, and D. Vlassopoulos, "Perspectives on the viscoelasticity and flow behavior of entangled linear and branched polymers," *J. Phys.: Condens. Matter* **27**(47), 473002 (2015).
- [28] Marrucci, G., "Dynamics of entanglements: A nonlinear model consistent with the Cox-Merz rule," *J. Non-Newtonian Fluid Mech.* **62**(2–3), 279–289 (1996).
- [29] Ianniruberto, G., and G. Marrucci, "Do repeated shear startup runs of polymeric liquids reveal structural changes?," *ACS Macro Lett.* **3**(6), 552–555 (2014).
- [30] Ianniruberto, G., and G. Marrucci, "Convective constraint release (CCR) revisited," *J. Rheol.* **58**(1), 89–102 (2014).
- [31] Cao, J., and A. E. Likhtman, "Shear banding in molecular dynamics of polymer melts," *Phys. Rev. Lett.* **108**(2), 28302 (2012).
- [32] Divoux, T., C. Barentin, and S. Manneville, "Stress overshoot in a simple yield stress fluid: An extensive study combining rheology and velocimetry," *Soft Matter* **7**(19), 9335–9349 (2011).
- [33] Boukany, P. E., and S.-Q. Wang, "Shear banding or not in entangled {DNA} solutions depending on the level of entanglement," *J. Rheol.* **53**(1), 73–83 (2009).
- [34] Thomas Hu, Y., L. Wilen, A. Philips, and A. Lips, "Is the constitutive relation for entangled polymers monotonic?," *J. Rheol.* **51**(2), 275–295 (2007).
- [35] Li, X., and S.-Q. Wang, "Elastic yielding after step shear and during LAOS in the absence of meniscus failure," *Rheol. Acta* **49**(10), 985–991 (2010).
- [36] Boukany, P. E., and S.-Q. Wang, "Exploring origins of interfacial yielding and wall slip in entangled linear melts during shear or after shear cessation," *Macromolecules* **42**(6), 2222–2228 (2009).
- [37] Wang, S.-Q., S. Ravindranath, P. E. Boukany, M. Olechnowicz, R. P. Quirk, A. Halasa, and J. Mays, "Nonquiescent relaxation in entangled polymer liquids after step shear," *Phys. Rev. Lett.* **97**(18), 187801 (2006).
- [38] Fang, Y., G. Wang, N. Tian, X. Wang, X. Zhu, P. Lin, G. Ma, and L. Li, "Shear inhomogeneity in poly(ethylene oxide) melts," *J. Rheol.* **55**(5), 939–949 (2011).
- [39] Ravindranath, S., and S.-Q. Wang, "What are the origins of stress relaxation behaviors in step shear of entangled polymer solutions?," *Macromolecules* **40**(22), 8031–8039 (2007).
- [40] Archer, L. A., Y. L. Chen, and R. G. Larson, "Delayed slip after step strains in highly entangled polystyrene solutions," *J. Rheol.* **39**(3), 519–525 (1995).
- [41] Boukany, P. E., and S.-Q. Wang, "Use of particle-tracking velocimetry and flow birefringence to study nonlinear flow behavior of entangled wormlike micellar solution: From wall slip, bulk disentanglement to chain scission," *Macromolecules* **41**(4), 1455–1464 (2008).
- [42] Gibaud, T., D. Frelat, and S. Manneville, "Heterogeneous yielding dynamics in a colloidal gel," *Soft Matter* **6**(15), 3482–3488 (2010).
- [43] Divoux, T., C. Barentin, and S. Manneville, "From stress-induced fluidization processes to Herschel-Bulkley behaviour in simple yield stress fluids," *Soft Matter* **7**(18), 8409–8418 (2011).
- [44] Thomas Hu, Y., C. Palla, and A. Lips, "Comparison between shear banding and shear thinning in entangled micellar solutions," *J. Rheol.* **52**(2), 379–400 (2008).
- [45] Thomas Hu, Y., and A. Lips, "Kinetics and mechanism of shear banding in an entangled micellar solution," *J. Rheol.* **49**(5), 1001–1027 (2005).
- [46] Thomas Hu, Y., "Steady-state shear banding in entangled polymers?," *J. Rheol.* **54**(6), 1307–1323 (2010).
- [47] Moorcroft, R. L., and S. M. Fielding, "Criteria for shear banding in time-dependent flows of complex fluids," *Phys. Rev. Lett.* **110**(8), 086001 (2013).
- [48] Moorcroft, R. L., and S. M. Fielding, "Shear banding in time-dependent flows of polymers and wormlike micelles," *J. Rheol.* **58**(1), 103–147 (2014).
- [49] Moorcroft, R. L., M. E. Cates, and S. M. Fielding, "Age-dependent transient shear banding in soft glasses," *Phys. Rev. Lett.* **106**(5), 055502 (2011).
- [50] Adams, J. M., S. M. Fielding, and P. D. Olmsted, "Transient shear banding in entangled polymers: A study using the Rolie-Poly model," *J. Rheol.* **55**(5), 1007–1032 (2011).
- [51] Manning, M. L., E. G. Daub, J. S. Langer, and J. M. Carlson, "Rate-dependent shear bands in a shear-transformation-zone model of amorphous solids," *Phys. Rev. E* **79**(1), 16110 (2009).
- [52] Marrucci, G., and N. Grizzuti, "The free energy function of the Doi-Edwards theory: Analysis of the instabilities in stress relaxation," *J. Rheol.* **27**(5), 433–450 (1983).
- [53] Fielding, S. M., R. L. Moorcroft, R. G. Larson, and M. E. Cates, "Modeling the relaxation of polymer glasses under shear and elongational loads," *J. Chem. Phys.* **138**(12), 12A504 (2013).
- [54] Jagla, E. A., "Shear band dynamics from a mesoscopic modeling of plasticity," *J. Stat. Mech.* **2010**(12), P12025.
- [55] Ravindranath, S., and S.-Q. Wang, "Steady state measurements in stress plateau region of entangled polymer solutions: Controlled-rate and controlled-stress modes," *J. Rheol.* **52**(4), 957–980 (2008).
- [56] Boukany, P. E., S.-Q. Wang, and X. Wang, "Step shear of entangled linear polymer melts: New experimental evidence for elastic yielding," *Macromolecules* **42**(16), 6261–6269 (2009).

- [57] Boukany, P. E., and S.-Q. Wang, "Exploring the transition from wall slip to bulk shearing banding in well-entangled DNA solutions," *Soft Matter* **5**(4), 780–789 (2009).
- [58] Hyun, K., M. Wilhelm, C. O. Klein, K. S. Cho, J. G. Nam, K. H. Ahn, S. J. Lee, R. H. Ewoldt, and G. H. McKinley, "A review of nonlinear oscillatory shear tests: Analysis and application of large amplitude oscillatory shear (LAOS)," *Prog. Polym. Sci.* **36**(12), 1697–1753 (2011).
- [59] Cohen, I., B. Davidovitch, A. B. Schofield, M. P. Brenner, and D. A. Weitz, "Slip, yield, and bands in colloidal crystals under oscillatory shear," *Phys. Rev. Lett.* **97**(21), 215502 (2006).
- [60] Dimitriou, C. J., L. Casanellas, T. J. Ober, and G. H. McKinley, "Rheo-PIV of a shear-banding wormlike micellar solution under large amplitude oscillatory shear," *Rheol. Acta* **51**(5), 395–411 (2012).
- [61] Kate Gurnon, A., and N. J. Wagner, "Large amplitude oscillatory shear (LAOS) measurements to obtain constitutive equation model parameters: Giesekus model of banding and nonbanding wormlike micelles," *J. Rheol.* **56**(2), 333–351 (2012).
- [62] Kate Gurnon, A., C. R. Lopez-Barron, A. P. R. Eberle, L. Porcar, and N. J. Wagner, "Spatiotemporal stress and structure evolution in dynamically sheared polymer-like micellar solutions," *Soft Matter* **10**(16), 2889–2898 (2014).
- [63] Wilhelm, M., "Fourier-transform rheology," *Macromol. Mater. Eng.* **287**(2), 83–105 (2002).
- [64] Tee, T.-T., and J. M. Dealy, "Nonlinear viscoelasticity of polymer melts," *J. Rheol.* **19**(4), 595–615 (1975).
- [65] Klein, C. O., H. W. Spiess, A. Calin, C. Balan, and M. Wilhelm, "Separation of the nonlinear oscillatory response into a superposition of linear, strain hardening, strain softening, and wall slip response," *Macromolecules* **40**(12), 4250–4259 (2007).
- [66] Klein, C., P. Venema, L. Sagis, and E. van der Linden, "Rheological discrimination and characterization of carrageenans and starches by Fourier transform-rheology in the non-linear viscous regime," *J. Non-Newtonian Fluid Mech.* **151**(1–3), 145–150 (2008).
- [67] Cho, K. S., K. Hyun, K. H. Ahn, and S. J. Lee, "A geometrical interpretation of large amplitude oscillatory shear response," *J. Rheol.* **49**(3), 747–758 (2005).
- [68] Ewoldt, R. H., A. E. Hosoi, and G. H. McKinley, "New measures for characterizing nonlinear viscoelasticity in large amplitude oscillatory shear," *J. Rheol.* **52**(6), 1427–1458 (2008).
- [69] Rogers, S. A., and M. Paul Lettinga, "A sequence of physical processes determined and quantified in large-amplitude oscillatory shear (LAOS): Application to theoretical nonlinear models," *J. Rheol.* **56**(1), 1–25 (2012).
- [70] Rogers, S. A., B. M. Erwin, D. Vlassopoulos, and M. Cloitre, "A sequence of physical processes determined and quantified in LAOS: Application to a yield stress fluid," *J. Rheol.* **55**(2), 435–458 (2011).
- [71] Zhou, Lin, Randy H. Ewoldt, L. Pamela Cook, and Gareth H. McKinley, "Probing Shear-Banding Transitions of Entangled Liquids Using Large Amplitude Oscillatory Shearing (LAOS) Deformations," *AIP Conf. Proc.* **1027**(1), 189–191 (2008).
- [72] Zhou, L., P. A. Vasquez, L. Pamela Cook, and G. H. McKinley, "Modeling the inhomogeneous response and formation of shear bands in steady and transient flows of entangled liquids," *J. Rheol.* **52**(2), 591–623 (2008).
- [73] Adams, J. M., and P. D. Olmsted, "Nonmonotonic models are not necessary to obtain shear banding phenomena in entangled polymer solutions," *Phys. Rev. Lett.* **102**(6), 067801 (2009).
- [74] Likhtman, A. E., and R. S. Graham, "Simple constitutive equation for linear polymer melts derived from molecular theory: Rolie-Poly equation," *J. Non-Newtonian Fluid Mech.* **114**(1), 1–12 (2003).
- [75] Graham, R. S., A. E. Likhtman, T. C. B. McLeish, and S. T. Milner, "Microscopic theory of linear, entangled polymer chains under rapid deformation including chain stretch and convective constraint release," *J. Rheol.* **47**(5), 1171–1200 (2003).
- [76] Lu, C.-Y. D., P. D. Olmsted, and R. C. Ball, "Effects of nonlocal stress on the determination of shear banding flow," *Phys. Rev. Lett.* **84**(4), 642–645 (2000).
- [77] Graham, R. S., E. P. Henry, and P. D. Olmsted, "Comment on 'New experiments for improved theoretical description of nonlinear rheology of entangled polymers'," *Macromolecules* **46**(24), 9849–9854 (2013).
- [78] Agimelen, O. S., and P. D. Olmsted, "Apparent fracture in polymeric fluids under step shear," *Phys. Rev. Lett.* **110**(20), 204503 (2013).
- [79] Larson, R. G., *Constitutive Equations for Polymer Melts and Solutions* (Butterworth, Stoneham, MA, 1988).
- [80] Press, W. H., S. A. Teukolsky, W. T. Vetterling, and B. P. Flannery, *Numerical Recipes in C* (Cambridge University, Cambridge, 1992).
- [81] Fujii, S., H. Morikawa, M. Ito, and T. Takahashi, "Transient behavior of stress in a wormlike micellar solution under oscillatory shear," *Colloid Polym. Sci.* **293**(11), 3237–3248 (2015).
- [82] Ewoldt, R. H., and G. H. McKinley, "On secondary loops in LAOS via self-intersection of Lissajous-Bowditch curves," *Rheol. Acta* **49**(2), 213–219 (2009).
- [83] Grand, C., J. Arrault, and M. E. Cates, "Slow transients and metastability in wormlike micelle rheology," *J. Phys. II* **7**(8), 1071–1086 (1997).
- [84] Fardin, M. A., C. Perge, L. Casanellas, T. Hollis, N. Taberlet, J. Ortin, S. Lerouge, and S. Manneville, "Flow instabilities in large amplitude oscillatory shear: A cautionary tale," *Rheol. Acta* **53**(12), 885–898 (2014).
- [85] Nghe, P., S. M. Fielding, P. Tabeling, and A. Ajdari, "Interfacially driven instability in the microchannel flow of a shear-banding fluid," *Phys. Rev. Lett.* **104**(24), 248303 (2010).
- [86] Fielding, S. M., "Linear instability of planar shear banded flow," *Phys. Rev. Lett.* **95**(13), 134501 (2005).
- [87] Fielding, S. M., "Viscoelastic Taylor-Couette instability of shear banded flow," *Phys. Rev. Lett.* **104**(19), 198303 (2010).
- [88] Milner, S. T., "Dynamical theory of concentration fluctuations in polymer solutions under shear," *Phys. Rev. E* **48**(5), 3674–3691 (1993).
- [89] Schmitt, V., C. M. Marques, and F. Lequeux, "Shear-induced phase separation of complex fluids: The role of flow-concentration coupling," *Phys. Rev. E* **52**(4), 4009–4015 (1995).
- [90] Fielding, S. M., and P. D. Olmsted, "Kinetics of the shear banding instability in startup flows," *Phys. Rev. E* **68**(3), 036313 (2003).
- [91] Fielding, S. M., and P. D. Olmsted, "Early stage kinetics in a unified model of shear-induced demixing and mechanical shear banding instabilities," *Phys. Rev. Lett.* **90**(22), 224501 (2003).
- [92] Skorski, S., and P. D. Olmsted, "Loss of solutions in shear banding fluids driven by second normal stress differences," *J. Rheol.* **55**(6), 1219–1246 (2011).
- [93] Berret, J.-F., G. Porte, and J.-P. Decruppe, "Inhomogeneous shear flows of wormlike micelles: a master dynamic phase diagram," *Phys. Rev. E* **55**(2), 1668–1676 (1997).